Real-Time Implementation of Single-Doppler Radar Analysis Methods for Tropical Cyclones: Algorithm Improvements and Use with WSR-88D Display Data

Paul R. Harasti[*]

National Center for Atmospheric Research,[+] Boulder, Colorado

Colin J. McAdie

NOAA/NWS/NCEP/Tropical Prediction Center, Miami, Florida

Peter P. Dodge

Hurricane Research Division, NOAA/AOML, Miami, Florida

Wen-Chau Lee and John Tuttle

National Center for Atmospheric Research,[+] Boulder, Colorado

Shirley T. Murillo and Frank D. Marks Jr.

Hurricane Research Division, NOAA/AOML, Miami, Florida

(Manuscript received 13 March 2003, in final form 18 August 2003)

ABSTRACT

The NOAA/NWS/NCEP/Tropical Prediction Center/National Hurricane Center has sought techniques that use single-Doppler radar data to estimate the tropical cyclone wind field. A cooperative effort with NOAA/Atlantic Oceanographic and Meteorological Laboratory/Hurricane Research Division and NCAR has resulted in significant progress in developing a method whereby radar display data are used as a proxy for a full-resolution base data and in improving and implementing existing wind retrieval and center-finding techniques. These techniques include the ground-based velocity track display (GBVTD), tracking radar echoes by correlation (TREC), GBVTD-simplex, and the principal component analysis (PCA) methods.

The GBVTD and TREC algorithms are successfully applied to the Weather Surveillance Radar-1988 Doppler (WSR-88D) display data of Hurricane Bret (1999) and Tropical Storm Barry (2001). GBVTD analyses utilized circulation center estimates provided by the GBVTD-simplex and PCA methods, whereas TREC analyses utilized wind center estimates provided by radar imagery and aircraft measurements. GBVTD results demonstrate that the use of the storm motion as a proxy for the mean wind is not always appropriate and that results are sensitive to the accuracy of the circulation center estimate. TREC results support a previous conjecture that the use of polar coordinates would produce improved wind retrievals for intense tropical cyclones. However, there is a notable effect in the results when different wind center estimates are used as the origin of coordinates. The overall conclusion is that GBVTD and TREC have the ability to retrieve the intensity of a tropical cyclone with an accuracy of ~ 2 m s^{-1} or better if the wind intensity estimates from individual analyses are averaged together.

1. Introduction

One of the mandates of the U.S. Weather Research Program (USWRP) is to support tropical cyclone (TC) research that may contribute to a reduction in their disastrous impacts on the nation (Elsberry and Marks 1998; Emanuel et al. 1995; Marks and Shay 1998). Better warnings would reduce the number of deaths and minimize the economic losses due to unnecessary evacuations. A major thrust in USWRP is to exploit new land-based technology in observations of the atmospheric boundary layer as the TC moves from ocean to land. The evolution and characteristics of the surface wind field and the vertical structure of the wind field before and after landfall need to be better diagnosed and understood in order to improve TC warnings and forecasts. The network of Weather Surveillance Radar-1988

Doppler (WSR-88D) units in the United States and abroad routinely scan regions out to ~400 km range roughly every 6 min and are therefore ideally suited for monitoring TCs that track near the coastline. However, researchers have had to rely on *single*-Doppler radar wind retrieval techniques to deduce the TC wind field because the distances between radars is too large to permit adequate dual-Doppler radar wind analyses. Lee et al. (1999, hereafter LJCD), Lee and Marks (2000), and Lee et al. (2000) demonstrated that the wind field could be retrieved reasonably well by the ground-based velocity track display (GBVTD) method. Similarly, Tuttle and Gall (1999, hereafter TG) successfully retrieved TC winds with the tracking radar echoes by correlation (TREC) method.

A cooperative effort among the National Center for Atmospheric Research, the National Oceanic and Atmospheric Administration (NOAA)/Atlantic Oceanographic and Meteorological Laboratory (AOML)/Hurricane Research Division (HRD) and NOAA/National Weather Service (NWS)/National Centers for Environmental Prediction (NCEP)/Tropical Prediction Center (TPC)/National Hurricane Center (NHC) has led to the improvement and real-time implementation of the GBVTD and TREC methods. However, this effort has met significant obstacles. Owing to the technological limitations of the early 1980s, the design emphasis of the WSR-88D was on remote display, not remote processing. As a consequence, TPC and other NCEP forecast centers have not had real-time access to full-volume, full-precision base data. Base data include reflectivity, Doppler velocity, and spectrum width, and these quantities are archived together into data files referred to as ''level II'' data. The new ''open system'' architecture of the WSR-88D Radar Product Generator (RPG) has made the availability of real-time base data at NCEP a reality for the near future (Crum et al. 1998). The Collaborative Radar Acquisition Field Test (CRAFT; Droegemeier et al. 2002) has already developed a network system that has steadily increased the number of WSR-88D units delivering real-time base data to government, university, and private sectors. However, it has been necessary to utilize an alternative to base data along the way since very few WSR-88D units in regions prone to TCs have as yet been included in the CRAFT project.

The alternative data that are available to NCEP in real time are meteorological analysis products generated from the base data, which are stored in a digital format known as ''level III'' or ''level IV'' data (Crum et al. 1993). The specific products that are of use to GBVTD and TREC are display products of reflectivity and Doppler velocity (hereafter, display data). Each display data file contains information to construct a contour map showing one of these data types around a single, 360° azimuthal scan at constant elevation angle [referred to as a plan position indicator (PPI) scan in the lexicon of radar meteorology].
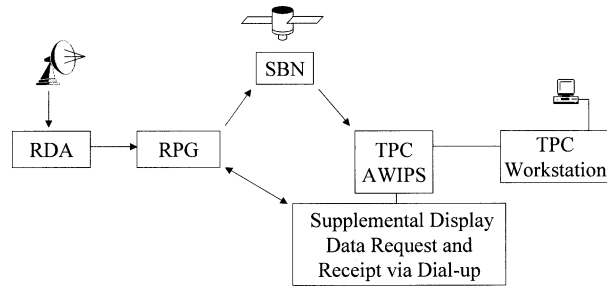

FIG. 1. The flow of WSR-88D display data to TPC. The display data are generated from the base data at the RPG, which are in turn derived from the raw analog data gathered at the Radar Data Acquisition (RDA) site. Display data files are transferred automatically from the RPG to AWIPS via SBN. An AWIPS user may also request supplemental display data from a specific radar site via dial-up to its RPG. The display data are sent from AWIPS to a TPC workstation where the various algorithms are located.

There have been obstacles concerning display data as well. Display data have been available in real time via the Next-Generation Weather Radar (NEXRAD) Information Dissemination Service (NIDS) vendors (Baer 1991). However, products specifically needed for TC applications, such as the eight-contour-level Doppler velocity product described in the next section, have not been made available by the distributors. Therefore, it has been necessary for TPC to devise its own means to acquire the display data that it requires. Prior to the recent replacement of the Principal User Processor (PUP) with the Advanced Weather Interactive Processing System (AWIPS) at TPC, any display data missing from the NIDS data suite were captured from the PUP in real time using computer hardware and software provided by L. Delemarre of the Federal Aviation Administration (McAdie et al. 2001).

The objectives of this paper are to 1) describe how display data can be used as a proxy for base data in the context of GBVTD and TREC, 2) describe improvements to the GBVTD and TREC methods, and 3) present results from two TC case studies. Section 2 describes the current data acquisition method using AWIPS and the processing of display data. Improvements to the GBVTD and TREC techniques are presented in section 3 along with a description of required center-finding methods. Section 4 shows the results of the applications of the improved GBVTD and TREC algorithms to the WSR-88D display data of Hurricane Bret (1999) and Tropical Storm Barry (2001). A summary and conclusions are presented in section 5.

2. The acquisition and processing of display data

AWIPS at TPC receives the first elevation angle PPI display data automatically in real time from the Satellite Broadcast Network (SBN). Figure 1 shows a diagram of the flow of display data to TPC. An AWIPS user may also request supplemental display data from a specific radar site via dial-up to its RPG. TPC requests the

TABLE 1. Relationship between full-resolution base Doppler velocity data (V_D) and its corresponding display data contour level and TREC data value. TREC data values are assigned the midpoint value of their corresponding V_D range (except at the upper and lower velocity bounds) to increase the overall accuracy of Doppler velocity estimates of radar echoes located in the regions between the displayed contour level boundaries. All units are in m s^{-1}.

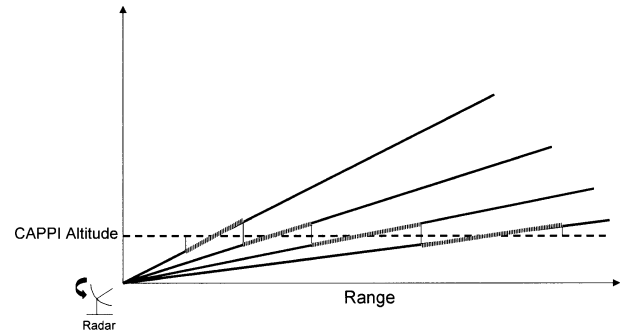| Base Doppler velocity value range	Display data contour level	TREC data value
Not detectable	Not detectable	Not detectable
$V_D \leq -33$	-33	-33
$-33 < V_D \leq -26$	-26	-29.5
$-26 < V_D \leq -19$	-19	-22.5
$-19 < V_D \leq -13$	-13	-16
$-13 < V_D \leq -10$	-10	-11.5
$-10 < V_D \leq -5$	-5	-7.5
$-5 < V_D \leq -1$	-1	-3
$0 \leq V_D < 5$	0	2.5
$5 \leq V_D < 10$	5	7.5
$10 \leq V_D < 13$	10	11.5
$13 \leq V_D < 19$	13	16
$19 \leq V_D < 26$	19	22.5
$26 \leq V_D < 33$	26	29.5
$V_D \geq 33$	33	33
Range ambiguous	Range ambiguous	Range ambiguous

FIG. 2. A simplified schematic of the original CAPPI construction proposed by Marshall (1957). The horizontal and vertical axes show the horizontal range and altitude, respectively, measured from the radar. In this example, the radar at the lower left scans through four successive PPI scans at four different elevation angles. The four solid lines represent four radar beams found at the same azimuth angle within the four PPI scans. A quasi-horizontal CAPPI map is produced at a user-specified altitude by combining the appropriate sections (hashed lines) of each radar beam around 360° of azimuth. The individual sections are chosen so that the selected altitude bisects them, and they meet each other without leaving gaps or overlaps. The standard 4/3 earth radius model is used to correct the altitude of the radar beam sections for atmospheric refraction and the earth's curvature. Unlike conventional CAPPI maps interpolated to Cartesian coordinates, the coordinates of each datum in the Marshall CAPPI map remain expressed in radar–polar coordinates.

display data for the second through fifth elevation angle PPI scans that are missing from the SBN. Although AWIPS can receive any desired display data via the dial-up, in practice we have found that only up to the first five elevation angle PPI scans can be obtained reliably in real time (primarily a communications bandwidth issue). The display data are sent from AWIPS to a TPC workstation where the various algorithms are located.

The range and azimuthal resolution of the display data are 1 km and 1°, respectively. The precision of the display data is defined by the *increment* in either 16 or 8 contour levels corresponding to the familiar color-coded legend in a contour map of a single PPI scan. For example, Table 1 shows the typical 16 contour levels used for the display data of Doppler velocity along with the range of full-resolution base data that each contour level represents. The base data are stratified into the ranges shown in column 1 and then are assigned to 1 of a possible 14 contour levels; the remaining 2 contour levels are used to designate range ambiguous and nondetectable signals. Thus, the precision of display data is very coarse in comparison to base data, which have a precision of either 0.5 or 1 m s^{-1} for the case of Doppler velocity. It is possible to expand the upper- and lower-contour-level values in the Doppler velocity display to resolve TC winds in excess of 33 m s^{-1}; however, in order to prevent the degrading of the 16-contour-level product any further, an extra 8 contour levels are utilized instead. Base data converted to these eight extra contour levels are stored in a separate product file by the RPG. The particular contour levels used in the display data are specified in the WSR-88D Tropical Cyclone Operations Plan (see http://www.srh.noaa.gov/mlb/ntltcops.html for details). By comparison, the 16 contour

levels found in the display data files for reflectivity range from 5 to 75 dBZ in 5-dBZ increments, with one color level reserved for signals not detectable. This 5-dBZ precision is much coarser than the 0.5-dBZ precision of base reflectivity data.

The 16-contour-level display data files of reflectivity are collected in real time along with the 16- and 8-contour-level display data files of Doppler velocity. A composite data array is then made from the 16- and 8-contour-level Doppler velocity data at the beginning of the algorithms used at the TPC workstation. Occasionally, the RPG does not completely de-alias the base Doppler velocity before converting it to display data. The aliased data are identified in the Doppler velocity images and interactively reassigned to the contour level for signals not detectable in the algorithms. As a final data processing step, constant altitude PPI (CAPPI) maps of reflectivity and Doppler velocity are made from all the available PPI display data. Owing to the course precision of display data, the limited number of PPI scan elevation angles, and the small subset of display data used by GBVTD (to be discussed below), we have adopted the original CAPPI construction method proposed by Marshall (1957). As a review, Fig. 2 gives an example of this type of CAPPI construction. Unlike conventional CAPPI maps of base data interpolated to Cartesian coordinates (e.g., Mohr et al. 1986), the coordinates of each datum in the Marshall CAPPI map remain expressed in radar–polar coordinates. The GBVTD and TREC methods are applied to the CAPPI maps as follows.

GBVTD requires an accurate measure of the gradient

of the Doppler velocity in order to retrieve the asymmetries in the storm. This gradient is not detectable between the contour level boundaries displayed in the CAPPI maps where the Doppler velocity is constant according to the values shown in column 2 of Table 1. Therefore, the only parts of the display data used in the GBVTD algorithm are the radar–polar coordinates of the *boundaries* between the contour levels and their contour level values, with the exception of the contour level boundaries that involve range ambiguous data and signals not detectable, as well as those artificially generated in the CAPPI construction (i.e., the boundaries of the PPI sections that make up the CAPPI). In this way, only the areas in the display data that exactly equal the base data are utilized. This can be inferred from Table 1—note the correspondence of thresholds (equality values) in column 1 with the contour levels in column 2. This approach is an extension of the methods proposed by Houston et al. (1999) and McAdie et al. (2001) who applied GBVTD to PPI display data maps rather than CAPPI maps.

The exact Doppler velocity values along the contour level boundaries could be interpolated in the radar–azimuthal direction at all ranges from the radar with the use of a wavenumber-2 truncated Fourier series, such as the velocity–azimuth display (VAD) method of Browning and Wexler (1968); however, this approach is not expected to yield a sufficiently accurate gradient in the Doppler velocity for GBVTD. This follows from the work of Donaldson and Harris (1989) who showed that the wind speed is greatly underestimated by 20% or more when using the VAD method in the inner core of a TC where the wind field is strongly nonlinear. Harasti and List (2001b) showed that in fact 10 harmonics or more are necessary to sufficiently approximate the Doppler velocity in this region of a TC. Unfortunately, such an approximation would be biased if used in the current approach because the large azimuthal spacing between the contour level boundaries would create high-amplitude, high-frequency oscillations in the Fourier series fits (Gibbs phenomena). Thus, our use of only the contour level boundaries in the Doppler velocity for GBVTD would likely be the most prudent approach to the problem.

In contrast to GBVTD, the TREC algorithm at TPC utilizes *all* of the display data constituting the CAPPI maps of reflectivity and Doppler velocity. TREC has no choice but to use the data points in between the contour level boundaries because it calculates the winds from the motion of reflectivity echoes that extend between these boundaries. However, exact reflectivity values are not required in this case because the TREC correlations can still be computed from the echo patterns labeled with inexact reflectivity values. On the other hand, TREC does require accurate Doppler velocities everywhere in the radar domain, although perhaps not to the degree of accuracy as GBVTD requires, since inexact gradients are not a concern in this case. TPC has elected

to adjust the display data of Doppler velocity to the midpoint values of their corresponding base Doppler velocity ranges (Table 1). This is an efficient way to increase the overall accuracy of the Doppler velocity estimates for TREC everywhere in the domain, where a loss of accuracy at the contour level boundaries is offset, overall, by an increase in accuracy over the entire area spanned by the radar echoes.

3. Algorithm improvements and center-finding particulars

a. GBVTD

The GBVTD method provides an estimate of the horizontal winds of a TC relative to the mean wind vector ($\mathbf{V}_M$; magnitude, V_M) around rings concentric with the circulation center position. The mean wind around a GBVTD ring corresponds to the environmental wind, which is assumed to vary only with altitude across the inner core of the TC. Harmonic analyses of the Doppler velocity data are performed around the GBVTD rings, and the resulting Fourier coefficients are related to various wavenumber components of the tangential and radial wind that are intrinsic to the TC, including *one* component of $\mathbf{V}_M$. There are many ways that one can interpret the GBVTD solution since the system of equations is not closed. The current approach utilizes the closure assumptions of previous studies; namely, 1) the streamlines of the nondivergent component of the horizontal winds are nearly circular, and 2) the azimuthal asymmetries in the radial wind are negligible.

In order to increase their operational utility at TPC, the GBVTD winds are adjusted to a ground-relative frame of reference using a complete estimate of $\mathbf{V}_M$. In the GBVTD coordinate system, $\mathbf{V}_M$ is resolved into two components with respect to the direction of the radar beam that passes through the circulation center position; an along- and an across-beam component. However, GBVTD only provides an estimate of the along-beam component; therefore, the across-beam component must be estimated from an independent source. TPC has elected to use the across-beam component of the storm motion as a proxy for the across-beam component of the mean wind in the GBVTD algorithm. This proxy is also used to make a correction for the across-beam component of the mean wind found in the expression for the GBVTD wavenumber-0 component of the tangential wind:

$$V_{T0} = -B_1 - B_3 - V_M \sin(\theta_T - \theta_M) \sin(\alpha_{max}), \quad (1)$$

where B_1 and B_3 are Fourier coefficients derived from the Doppler velocity data taken from a particular GBVTD ring, θ_T and θ_M are the mathematical azimuth angles for the circulation center position and the direction of the mean wind, respectively, $V_M \sin(\theta_T - \theta_M)$ is the across-beam component of the mean wind, and $\sin(\alpha_{max}) = R/R_T$, where R is the range from the circulation center to the GBVTD ring, and R_T is the range

from the radar to the circulation center position. {See LJCD for details and note the correction to the sign of "B_3" [cf. Eq. (20) of LJCD and Eq. (1) above].} The last term on the right-hand side of (1) was ignored in the original formulation of GBVTD, but it is included in the current approach by using the mean-wind estimate and the estimate of the circulation center position (R_T, θ_T) (see section 3c for details). The correction for this term monotonically approaches 100% of V_M from the circulation center to the GBVTD ring whose circumference passes directly above the radar, for mean-wind directions that are largely in the across-beam direction (Fig. 11 of LJCD).

There are also some new processing techniques applied to the GBVTD method based on empirical and theoretical considerations:

1) Owing to the limited number of data, the GBVTD analysis is performed on all the contour level boundaries within 5-km-wide annuli centered on the circulation center. The midpoint radius of each annulus is positioned radially outward from the center in 1-km steps. Thus, the annuli are overlapping, and the GBVTD coefficients are estimated at each integer-number radius.
2) In order to limit the variance in the coefficients, GBVTD is only applied to those annuli containing a minimum of 10 contour-level boundary points.
3) Limits are also set on the maximum azimuthal gap between the contour-level boundary points within the annuli. These limits prevent instabilities in the Fourier harmonics of the GBVTD fit caused by Gibbs phenomena. Refer to LJCD Eqs. (13)–(27) for the relations between the Fourier harmonics and the various wavenumber components of the tangential and radial wind, and the along-beam component of the mean wind. The empirically determined limits that have been successful are maximum gaps of 60°, 90°, 120°, and 150° for the Fourier harmonic wavenumbers 4, 3, 2, and 1, respectively.
4) The limits on sin (α_{max}) for the various wavenumber components discussed in LJCD are simultaneously imposed with the limits in 3 above in order to minimize the potential bias in the GBVTD wind results to 20%. Since the sin (α_{max}) limits are most restrictive for wavenumber components greater than 1, the GBVTD wind results shown in this paper only include wavenumber components *up to* wavenumber 1.
5) The GBVTD-estimated wind components are smoothed using 5-km running averages in the radial direction.

b. TREC

TREC was first developed to determine internal motions of storms by Rinehart and Garvey (1978) and was later modified by Tuttle and Foote (1990) for boundary layer studies. Tuttle and Gall (1999) used TREC to es-

timate winds from the motions of reflectivity echoes as they circulated around the eye in three TCs of differing intensities. The key assumption in TREC is that the features being tracked act as passive, conservative tracers that advect with the local winds with no sources or sinks (evaporation, condensation, microphysical processes, strong vertical motions). These conditions, of course, can never be strictly satisfied, but as long the sampling time between scans of the same elevation angle (~6 min) is significantly less than the typical lifetime of an ordinary cell (~30 min), then the assumption is approximately valid.

In brief, the original Cartesian coordinate version of TREC works as follows. The reflectivity data from two consecutive PPI scans of the same elevation angle are stored. The first scan is divided into a number of equal-sized two-dimensional arrays of data (21 km on a side) spaced apart by a distance equal to the chosen grid spacing. Each initial array is compared with all possible arrays of the same size in the second scan to find the best matching second array that has the highest correlation coefficient. The location of the second array determines the endpoint of the estimated wind vector. To help reduce errors due to strong temporal evolution, vectors with correlations less than a threshold (typically set to 0.3–0.4) are discarded. As a final step, TG recommended replacing the radar-radial component of the TREC winds with the Doppler velocity in the vicinity of the initial array position.

In most situations TG found good agreement between the TREC results and aircraft/Doppler measurements; however, several possible sources of error were mentioned. TREC often produced poor results near the eyewall and outer rainbands of the more intense TCs. This was in large part due to the fairly uniform reflectivity structure (in the direction of airflow) found in these regions. It should be emphasized that this uniform reflectivity is not necessarily visible as a lack of texture in the displays of reflectivity but rather mathematically as a region where the correlation field is broad and lacking curvature. Therefore, in order for the TREC technique to work well in most areas of the TC, the size of the correlation arrays must be large enough that the reflectivity has curvature over the array dimensions. This means that the array size needs to be about one-half the scale size of the reflectivity features or larger, otherwise, there may be large uncertainties in the endpoints of the wind vectors. The use of coarse-resolution display data of reflectivity in the current application only exacerbates this problem by reducing the likelihood of finding curvature in the reflectivity structure. Another source of error is the large radial wind shear in the vicinity of the eyewall leading to differential echo motion across the correlation box. To help alleviate these problems, TG proposed doing the analysis on a polar grid centered on the TC eye using arc-shaped (range–azimuth) correlation areas with the shorter dimension in the range direction (direction of maximum wind

shear) and the longer dimension in the azimuthal direction (the direction most likely to have uniformity in reflectivity in the eyewall or rainbands). This polar coordinate version has been implemented along with the original Cartesian coordinate version of TREC at TPC.

The polar coordinate version of TREC interpolates the reflectivity and Doppler velocity data to a polar grid of 1 km and 1° spacing using a simple closest point method and the apparent wind center as the origin. The wind center can be estimated from reflectivity/Doppler velocity methods or aircraft data (see section 3c for details). The dimensions of the correlation array are set to 12 km in range and 45° in azimuth, and the search for the best correlation match is limited to the cyclonic direction for TCs in the Northern Hemisphere and to the anticyclonic direction for TCs in the Southern Hemisphere. These search direction limitations of the polar coordinate version of TREC make it computationally faster than the Cartesian coordinate version of TREC. The position and vector coordinates of the estimated winds are expressed in a Cartesian coordinate system of specified grid spacing. However, the searches for the endpoints of the wind vectors are conducted in polar coordinates, commencing from the sector-shaped correlation arrays closest to the Cartesian grid points.

After the wind vector field has been computed, a two-dimensional, nearest-gridpoint, median smoother is used to remove outliers in the individual Cartesian components. In addition, although TG suggested that TREC be performed on the data taken from two consecutive (within ~6 min) PPI scans of the same elevation angle, TREC can also be implemented using two consecutive CAPPI maps instead. When utilized, this option increases the operational utility of TREC since wind diagnoses are more operationally useful when described for a constant altitude.

c. Center-finding requirements and methods

It is important at this point to clearly define what is meant by the terms "circulation center" and "wind center" and to explain why these two different center estimates are necessary in different situations and how they are determined. If the streamlines of the nondivergent component of the horizontal winds are nearly circular, and there is a single dynamic center within the eye of the TC, the circulation center is located at the center of the swirling wind in the mean-wind frame of reference. The wind center, on the other hand, is located at the center of the swirling wind observed in the ground's frame of reference. Depending on the magnitude of the mean wind, the circulation and wind centers are typically offset from each other by a few to several kilometers (idealized examples of their relative locations are shown in Fig. 5 of LJCD). GBVTD requires the winds to be resolved with respect to the circulation center because it estimates the swirling wind relative to the mean wind. Conversely, the polar coor-

dinate version of TREC requires the winds to be resolved with respect to the wind center because it estimates the swirling wind relative to the ground.

Historically, the operational goal of center finding has been to find the wind center since it is estimated by aircraft, ship, radar, and other ground-relative measurements for use in TC forecast products and models. During TC events, the wind center is estimated at the TPC/NHC using imagery of the radar display data sent to AWIPS approximately twice an hour. This is accomplished by visually finding a point on the PPI maps that is nearest to the apparent center of the swirling wind in the animated reflectivity maps while closely coinciding with the zero isodop in the Doppler velocity maps. The TPC/NHC operational radar fix of the wind center is referred to as "NHC_FIX" in the following.

Now that the GBVTD method is being tested in real time at TPC, algorithms that specifically estimate the circulation center are also being tested. Two methods have been implemented in real time: the GBVTD-simplex method (hereafter, simplex) of Lee and Marks (2000) and the principal component analysis (PCA) center-finding technique of Harasti (2000). Simplex is an extension of GBVTD; therefore, its results pertain to the mean-wind frame of reference. The data processing involved in PCA filters out the mean wind so its results also pertain to the mean-wind frame of reference. Thus, the center of the swirling wind estimated by both simplex and PCA is a measure of the position of the circulation center. Both simplex and PCA find the center of the swirling wind by locating the position of the ring of maximum winds since it is the most readily found of all rings that are concentric with the circulation center.

Simplex finds the ring of maximum winds by searching for a point, over a range of distances from that point, where the calculated V_{T0} is a maximum at some radius of maximum wind (RMW). After initial estimates of the circulation center position and the RMW are provided, V_{T0} is calculated iteratively from (1). The initial estimate of the circulation center is approximated by the nearest operational fix of the wind center, or by the previous simplex estimate, if available. There can be a large scatter in the simplex results for different initial center guesses when there are significant gaps in the display data. To alleviate this problem, 25 initial center positions are chosen over a 12 km × 12 km grid centered on the initial circulation center guess. Then, the average simplex circulation center is calculated after outliers that deviate by more than two standard deviations are rejected. The RMW is either estimated from aircraft reconnaissance information, when available, or by measuring the distance from the operational fix of the wind center to the apparent eyewall of the TC shown in display data of reflectivity. For each of the 25 initial center guesses, the simplex search is performed within the range RMW $\pm \Delta R$, where $\Delta R = 0.2$ RMW. If this range of estimated RMWs does not include the true RMW, there may be no simplex solution, and a refined

RMWs guess may be required. The disadvantages of simplex are that it is not expected to perform as well when there is a small variation in the tangential wind magnitude with radius (relatively flat profile), and when there is significant missing data. However, the advantages of simplex are that it gives GBVTD its own built-in circulation center estimate and it can be run automatically on a sequence of consecutive CAPPI maps after its parameters are initialized with the necessary independent information at the beginning of the run.

PCA finds the ring of maximum winds by recognizing patterns similar to analytic TCs in the data. It uses the *entire* display data of Doppler velocity taken from a single PPI or CAPPI map and works in the radar–polar coordinate system. First, the data are centered along the radar–range direction—this step removes the radar–radial components of the mean wind from the Doppler velocity. Next, the covariance matrix of the map is formed and its corresponding eigenvectors and principal components are calculated. The eigenvectors have coefficients that are functions of the azimuth coordinates whereas the principal components have coefficients that are functions of the range coordinates. Eigenvector and principal component coefficients plotted against their coordinates often reveal physical relationships hidden in the data (e.g., Stidd 1967). The current approach involves a search for two readily identified cusps in the plots of one automatically located eigenvector and its corresponding principal component. The range and azimuth coordinates of the cusps locate the position of the ring of maximum winds. Harasti (2000) established this geometric link by applying PCA to synthetic radar datasets of a wide variety of analytic TCs. The disadvantage of PCA is that it is currently only semiautomated. However, it yields an estimate of the circulation center position and the RMW as frequently as the WSR-88D volume scans (~5 min). The advantages of PCA are that it does not require initialization parameters, it is robust against missing data, and it performs well for typical radial profiles of the swirling wind (e.g., Willoughby and Rahn 2002), including those that are flat.

Previous investigators have realized the importance of having an accurate estimate of the circulation center when decomposing the TC circulation in the wavenumber domain (e.g., Willoughby 1992; Marks et al. 1992). Lee and Marks (2000) illustrated that the error in the retrieved GBVTD asymmetric circulation is greater than 20% if the error in the estimated circulation center exceeds 1 km. Synthetic radar datasets of analytic TCs have suggested an accuracy of ~300 and ~500 m for simplex and PCA, respectively. Lee and Marks (2000) also showed that simplex often provided a precision of 1 to 2 km in circulation center estimates of Typhoon Alex (1987). Similarly, the precision of circulation center estimates from PCA has ranged from 1 to 2 km in case studies of Typhoon Alex (1987) and Hurricanes Erin (1995) and Bret (1999) (Harasti and
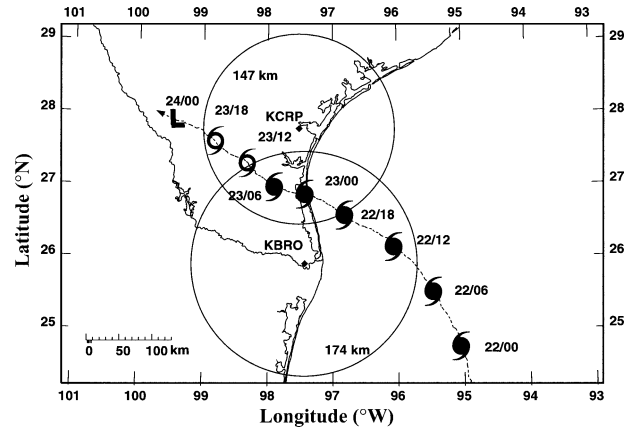

FIG. 3. The official best track of Hurricane Bret (dashed line) as it made landfall midway between KCRP and KBRO on the evening of 22 Aug 1999. Solid- and outlined-black hurricane symbols indicate hurricane and tropical storm intensity phases, respectively, and the "L" indicates a tropical depression. Numbers shown beside the symbols indicate the day in Aug and the time in hours (UTC). The solid circles indicate the de facto Doppler velocity range folding limits that are set by each radar's pulse repetition frequency: 147 and 174 km for KCRP and KBRO, respectively.

List 2001a). All of these case studies involving simplex and PCA utilized full-resolution base data, or the like—the current study is the first attempt at utilizing display data.

Consistency checks between the independent simplex and PCA estimates in real time provide a measure of confidence in the results, and the PCA estimate can be used along with simplex in GBVTD to yield a range of possible wind fields along with those obtained from TREC. The polar coordinate version of TREC utilizes either the NHC_FIX or aircraft reconnaissance estimates of the wind center, depending on the altitude of the analysis. The Cartesian coordinate version of TREC does not require an estimate of the wind center since its origin of coordinates is located at the radar.

4. Applications

a. Hurricane Bret (1999)

Hurricane Bret was a category 4 hurricane before it weakened to a category 3 hurricane a few hours before landfall along the Texas coast on 22 August 1999. Two WSR-88D coastal radars located at Corpus Christi (KCRP) and Brownsville (KBRO), Texas, made simultaneous observations of Bret. Figure 3 shows the official best track of Bret as it made landfall midway between KCRP and KBRO. The operational GBVTD and TREC algorithms were applied in poststorm analyses to display data of KCRP and KBRO as a proof of concept that CAPPI maps of display data could be successfully used with these algorithms. The display data were generated artificially from archived level II data using software that duplicates the RPG conversion of base data to dis-
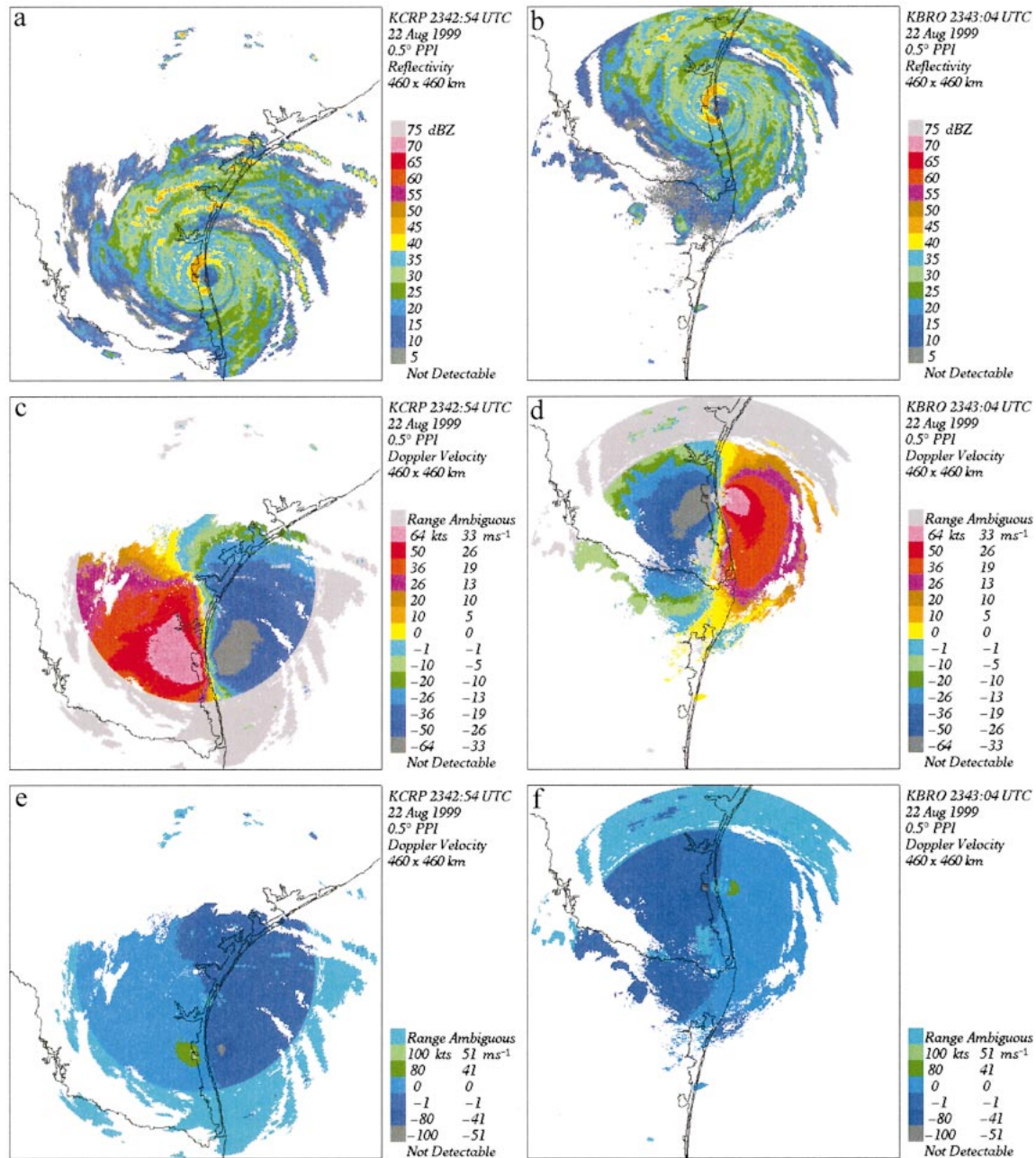
FIG. 4. PPI display data at 0.5° elevation showing Hurricane Bret as observed by (left) KCRP at 2342:54 UTC and (right) KBRO at 2343:04 UTC. (a), (b) The 16-contour-level reflectivity; (c), (d) the 16-contour-level Doppler velocity; and (e), (f) the 8-contour-level Doppler velocity. The particular radar is located at the center of each 460 km × 460 km domain.

play data (software provided by P. Jendrowski, Honolulu Weather Forecast Office). This was necessary because only the lowest-elevation display data had been archived at TPC during Hurricane Bret, an event that occurred prior to the use of CAPPI maps with GBVTD and TREC. Figure 4 shows the 16-contour-level reflectivity along with the 16- and 8-contour-level Doppler velocity derived from the lowest PPI scan taken at 0.5° elevation for both KCRP and KBRO at 2342:54 and 2343:04

UTC. Note that the 8-contour-level Doppler velocity really only includes four extra velocity levels (± 41 and ± 51 m s^{-1} in this particular case) since the 0 and -1 m s^{-1} contour levels are repeated. Figures 5a,b and 5e,f show 1.5-km CAPPI maps of reflectivity and Doppler velocity derived from the five lowest PPI scans of the KCRP and KBRO display data. Figures 5c,d show the 2.25-km CAPPI maps derived from the same KBRO PPI display data. Overall, the Marshall (1957) method
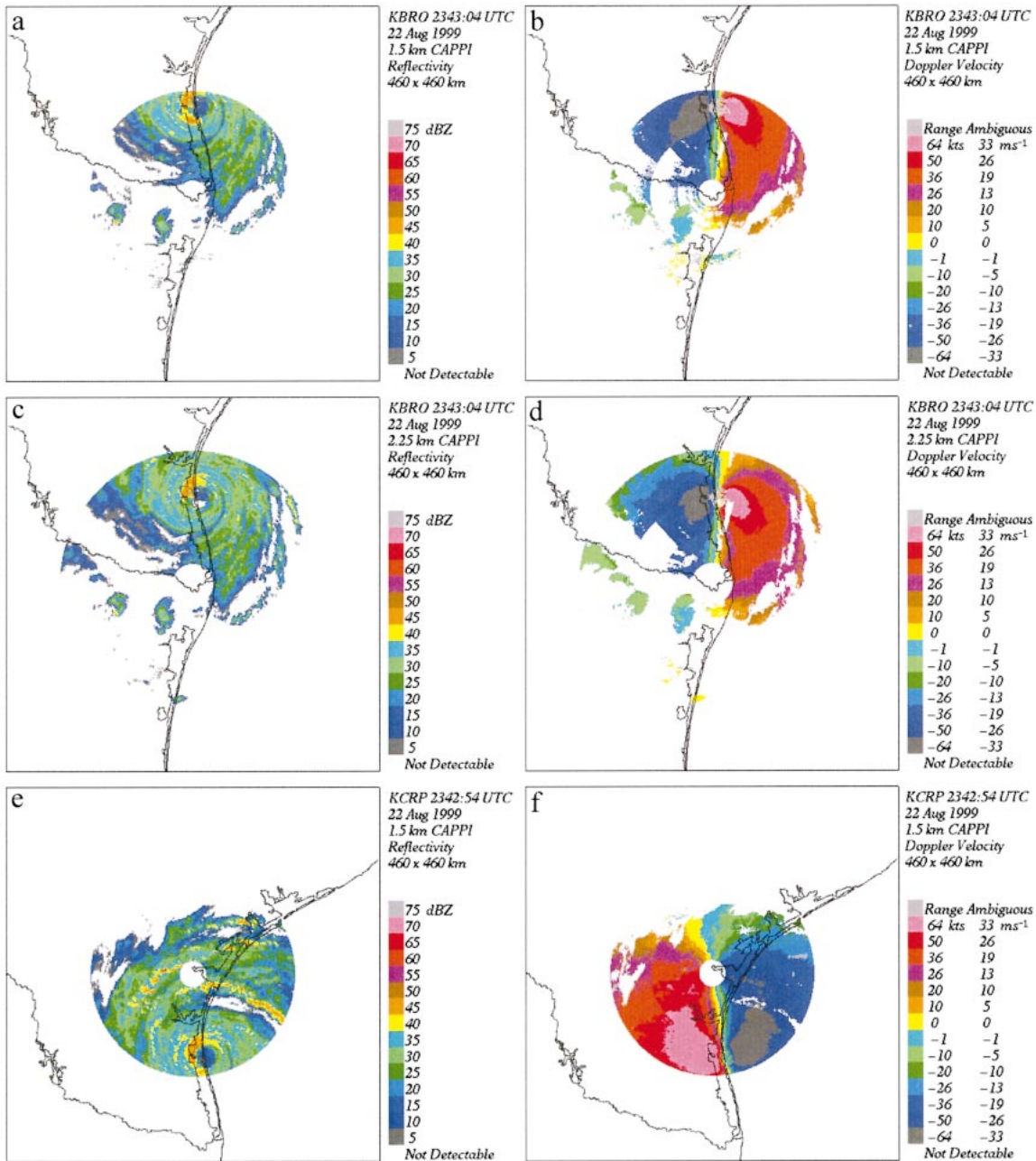
FIG. 5. The 16-contour-level CAPPI maps derived from the display data of the five lowest PPI scans taken at 0.5°, 1.5°, 2.5°, 3.5°, and 4.5° elevation: (a) 1.5-km CAPPI map of reflectivity derived from the KBRO data, (b) 1.5-km CAPPI map of Doppler velocity derived from the KBRO data, (c) 2.25-km CAPPI map of reflectivity derived from the KBRO data, (d) 2.25-km CAPPI map of Doppler velocity derived from the KBRO data, (e) 1.5-km CAPPI map of reflectivity derived from the KCRP data, and (f) 1.5-km CAPPI map of Doppler velocity derived from the KCRP data. The particular radar is located at the center of each 460 km × 460 km domain.

represents the data well, with only a few discontinuities in the Doppler velocity visible where the individual PPI annuli that constitute the CAPPI meet.

Figure 6a shows all of the available center estimates of Hurricane Bret relative to the NHC_FIX of Bret at 2342:54 UTC. Table 2 shows the specific coordinates of each center estimate. The NHC_FIX was estimated from the PPI display data sent to TPC from the KCRP

RPG. Since NHC_FIX was approximately 102 km away from KCRP, its approximate altitude along the 0.5° PPI was 1.5 km. Also shown in Fig. 6a is the Air Force reconnaissance wind center estimate (AF_RECON) taken at 2.6-km altitude at 2341:00 UTC, along with the PCA and simplex circulation center estimates at 1.5-km altitude from KCRP and KBRO at 2342:54 and 2343: 04 UTC, respectively (hereafter, PCA_KCRP, SIM-
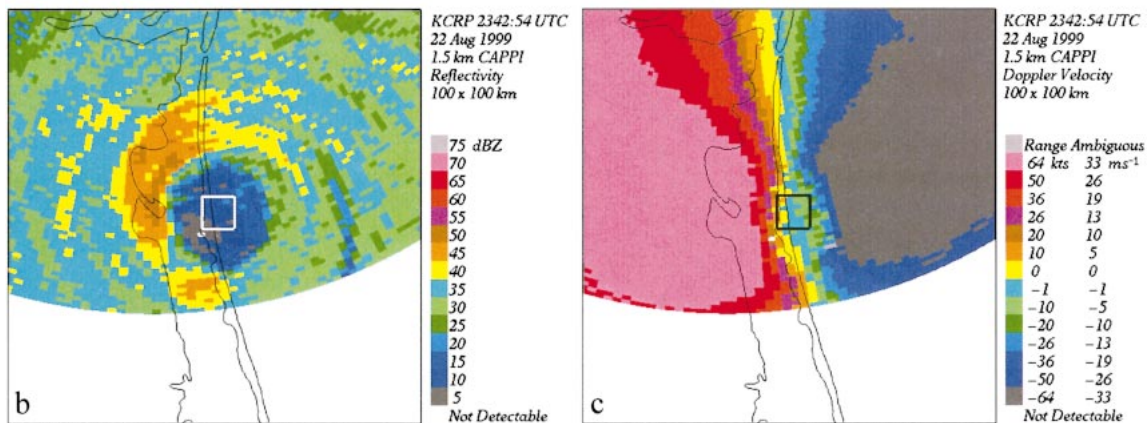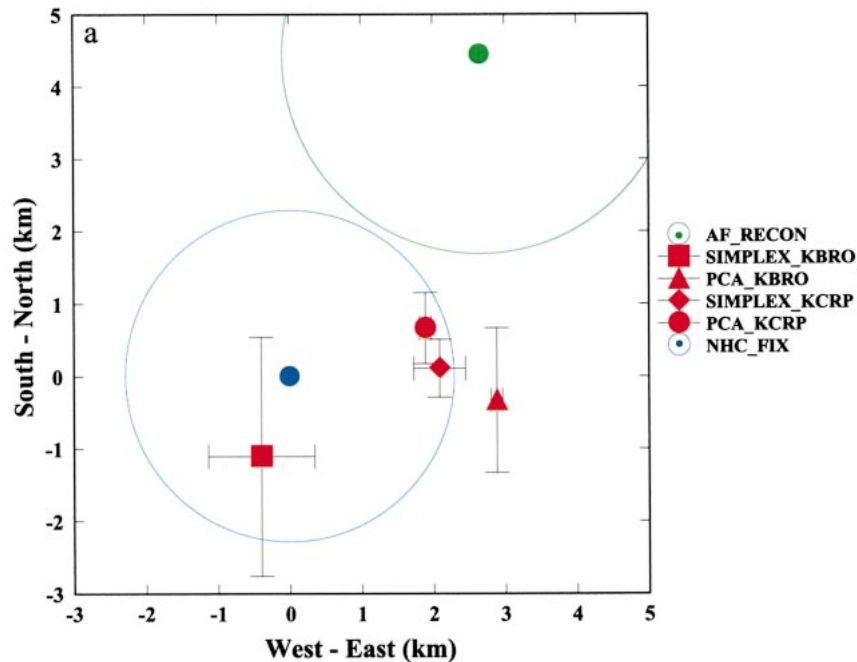
FIG. 6. (a) The center estimates available for Hurricane Bret relative to NHC_FIX at 2342:54 UTC. Circulation center estimates are shown as red symbols and black error bars, with labels shown in the legend indicating the technique used and the radar data source (KCRP or KBRO). Wind center estimates are shown as blue and green solid circles either partially or fully circumscribed by circles of the same color representing the approximate extent of their uncertainties. The approximate altitude of all the estimates is 1.5 km, except the AF_RECON estimate, which is at 2.6 km. (b), (c) Enlargements of Figs. 5e and 5f with horizontal limits 100 km × 100 km centered on NHC_FIX and with the location of the perimeter of (a) delineated by a white and black square, respectively.

PLEX_KCRP, PCA_KBRO, and SIMPLEX_KBRO). PCA was applied to composites of the 0.5° elevation, 16- and 8-contour-level Doppler velocity data (Figs. 4c–f). Simplex was applied to the 1.5-km CAPPI maps of Doppler velocity and utilized an initial RMW estimate of 18 km and the NHC_FIX as the initial center. Figure 6a also shows estimates of the uncertainty associated with each center estimate. The error bars for the simplex and PCA estimates correspond to the 95% confidence limits and the eigenvector analysis uncertainty, respec-

tively. The uncertainty circle for the AF_RECON wind center equals the sum of the navigational and meteorological uncertainties quoted in the Vortex Data Message that was sent to TPC/NHC. The NHC_FIX uncertainty circle is a rough estimate of the circular range of error perceived to be possible while attempting to locate the wind center from the radar display data. All uncertainty estimates *do not* include the unknown bias that *may* exist because of violations of the underlying assumption made for each technique. Figures 6b,c show

TABLE 2. The estimated positions of the circulation and wind centers discussed in this paper. All center estimates are quoted with a precision consistent with their uncertainties shown in Figs. 6a and 11c. Center estimate types are delineated either by W, for wind, or C, for circulation.

Tropical cyclone	Center position measurement/calculation	Lat (°N)	Lon (°W)	Center type	Alt ASL (km)
Hurricane Bret	NHC_FIX	26.86	97.36	W	1.5
(1999)	AF_RECON	26.900	97.333	W	2.6
	SIMPLEX_KCRP	26.861	97.339	C	1.5
	PCA_KCRP	26.866	97.341	C	1.5
	SIMPLEX_KBRO	26.850	97.364	C	1.5
	PCA_KBRO	26.857	97.331	C	1.5
Tropical Storm Barry	CAPPI_FIX	29.85	86.30	W	3.0
(2001)	AF_RECON	29.883	86.300	W	3.0
	SIMPLEX	29.850	86.267	C	3.0
	PCA	29.854	86.231	C	3.0

the perimeter of Fig. 6a superimposed on enlargements of Figs. 5e,f; the area of the enlargements corresponds approximately to the regions of the analyses shown in Figs. 7–9 and (later in) Fig. 11.

A pseudo-triple-Doppler radar wind analysis was performed on Hurricane Bret as a verification dataset for GBVTD and TREC. The analysis utilized NOAA P-3 aircraft Doppler radar data collected from 2323:04 to 2350:00 UTC 22 August 1999 during a research mission, along with the full-volume WSR-88D base data taken from KCRP and KBRO at 2342:54 and 2343:04 UTC, respectively (Dodge et al. 2002). A Cartesian coordinate system moving with the storm was defined using the NHC_FIX center position as the origin and a reference time of 2343:00 UTC. All the reflectivity and Doppler velocity data were interpolated to the Cartesian grid, then the variational technique of Gamache (1997)

was applied to yield an estimate of the three-dimensional wind field. Figure 7 shows the ground-relative wind speed at 1.5-km altitude derived from this technique. The mean wind over the 100 km × 100 km domain at this altitude was $(u_m, v_m) = (-7.1, -2.6)$ m s^{-1}, which was approximately twice the magnitude of the storm motion vector, $(u_s, v_s) = (-3.1, 1.8)$ m s^{-1}. These results are comparable to similar analyses at earlier times (Dodge et al. 2002) and are therefore considered reliable.

GBVTD was applied to the 1.5-km CAPPI maps of Doppler velocity at 2342:54 and 2343:04 UTC. Figure 8 shows the GBVTD results derived from KCRP using the SIMPLEX_KCRP (left) and PCA_KCRP (right) circulation centers. The first and second rows show the ground-relative GBVTD wind speed using the approximation $\mathbf{V}_M \approx (u_s, v_s)$ and $\mathbf{V}_M \approx (u_m, v_m)$, respectively.

2343:00 UTC 22 Aug 1999
Triple-Doppler Wind Speed
Ground Relative
1.5 km ASL
100 x 100 km
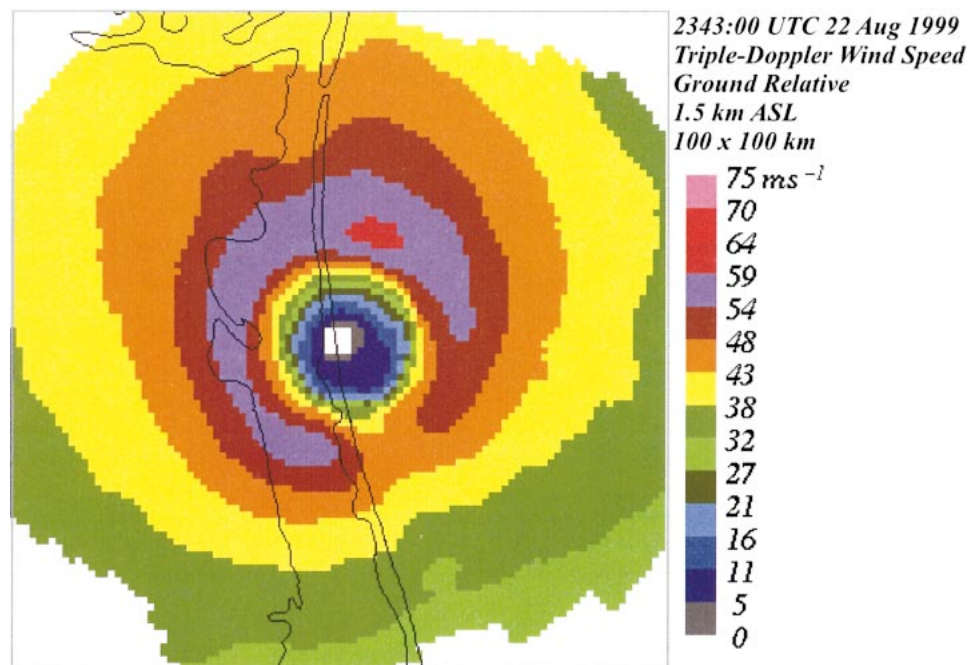
75 ms^{-1}
70
64
59
54
48
43
38
32
27
21
16
11
5
0

FIG. 7. Ground-relative wind speed of Hurricane Bret at 1.5-km altitude derived from a pseudo-triple-Doppler radar analysis, valid for 2343:00 UTC. The analysis is centered at NHC_FIX shown in Fig. 6a.
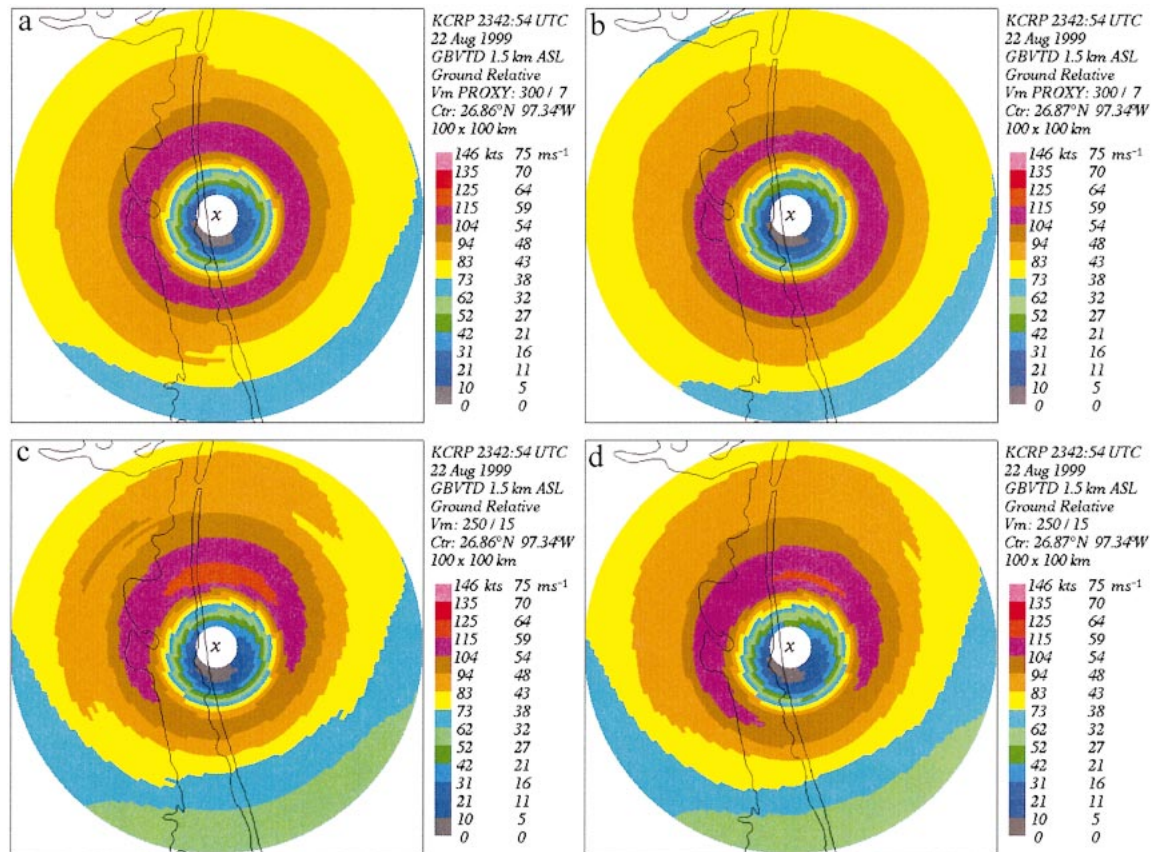
FIG. 8. GBVTD, ground-relative wind speed for Hurricane Bret at 1.5-km altitude above sea level (ASL), calculated from the KCRP CAPPI map and resolved with respect to the (left) SIMPLEX_KCRP and (right) PCA_KCRP circulation centers. (top) Results using the storm motion as a proxy for the mean wind, and (bottom) results using the mean wind. In each case, Eq. (1) has been used to correct V_{T0} for the across-beam component of the mean wind or its proxy, which is expressed as meteorological azimuth direction, and speed is in kt (7 kt ≈ 3.6 m s^{-1}; 15 kt ≈ 7.6 m s^{-1}). The area shown is 100 km × 100 km, centered on the particular circulation center, with the geographical boundaries overlain for comparison with Fig. 7. An ''x'' marks the location of the circulation center used (also shown in Fig. 6a).

The particular $\mathbf{V}_M$ was used in both (1) and in the transformation to the ground frame of reference. Figure 9 shows the same type of results except derived from the KBRO data using the SIMPLEX_KBRO (left) and PCA_KBRO (right) circulation centers.

The results shown in Figs. 8 and 9 demonstrate the sensitivity of the GBVTD retrieved winds to the circulation center used and the accuracy of the approximation $\mathbf{V}_M \approx (u_s, v_s)$. In order to study these two simultaneous effects separately, it is necessary to ascertain which of the circulation centers is most likely to be closest to the true circulation center at 1.5-km altitude. One way to accomplish this is to calculate the difference, ΔV_a, between the GBVTD-area-averaged and the pseudo-triple-Doppler-radar-area-averaged (ground truth) along-beam component of $\mathbf{V}_M$. If the underlying assumptions made by GBVTD are correct, the circulation center estimate closest to the true circulation center should show a GBVTD result $\Delta V_a \approx 0$ for both KCRP and KBRO because there is a bias in the *apparent* GBVTD along-beam component of $\mathbf{V}_M$ when the true circulation center position is not used in the GBVTD

calculations [see Table 1 of Lee and Marks (2000) for examples]. Table 3 shows the calculated ΔV_a values and their 99% confidence limits, specific to each of the four circulation center estimates available and each of the two radars. Hence, SIMPLEX_KCRP and PCA_KCRP are the most likely, and SIMPLEX_KBRO is the least likely, to be closest to the true circulation center based on the assumption $\Delta V_a = 0$. This conclusion is supported elsewhere in the results. First, Fig. 6a shows that the independent SIMPLEX_KCRP and PCA_KCRP estimates agree with each other to within their respective error bars, whereas SIMPLEX_KBRO and PCA_KBRO do not. Second, comparing Fig. 7 with Figs. 8c,d and 9c,d, we see the best agreement of results in Figs. 8c,d. Third, assuming SIMPLEX_KCRP and PCA_KCRP are very near the location of the true circulation center, Fig. 6a shows that both the SIMPLEX_KBRO and PCA_KBRO estimates are biased, probably because of the missing data within the eye of Bret shown by the range ambiguous data in Figs. 4d and 5b (which are not present in the KCRP data). In addition, the bias in PCA_KBRO appears to be significantly smaller than the
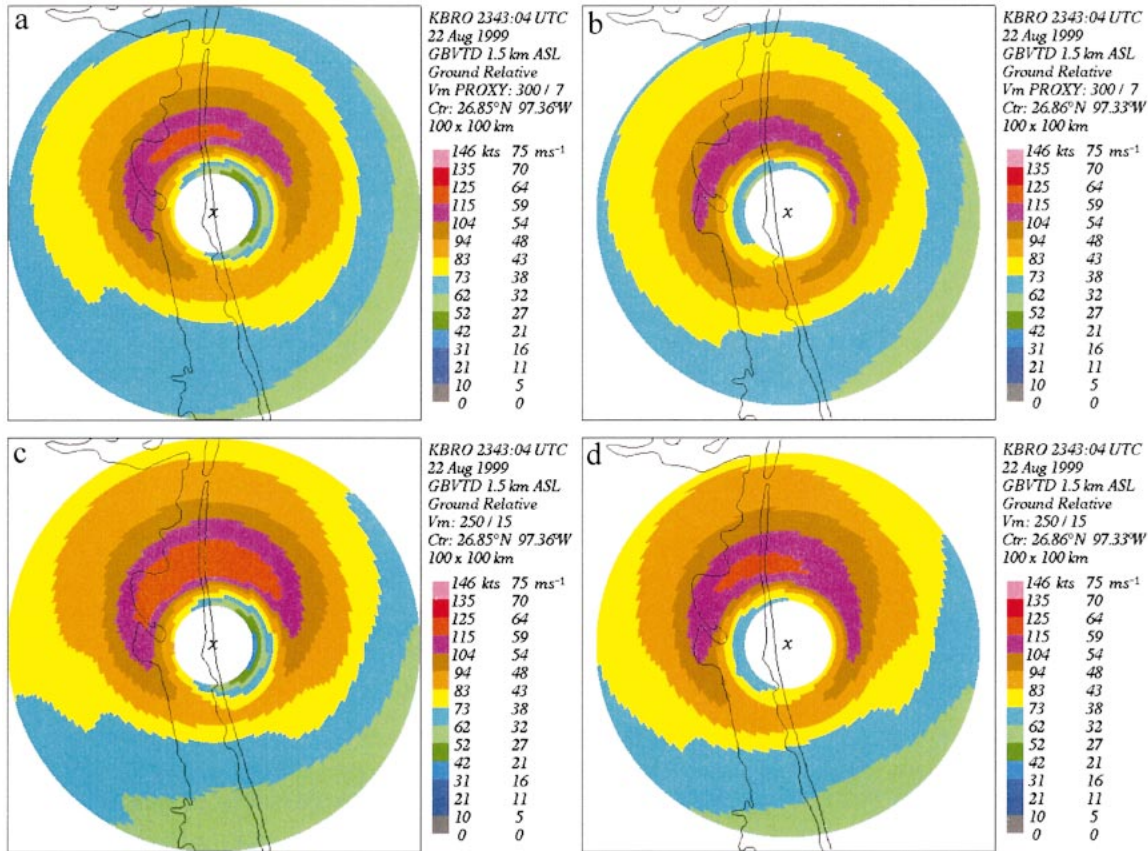
FIG. 9. Same as Fig. 8, except the GBVTD ground-relative wind speed for Hurricane Bret calculated from the KBRO CAPPI map and resolved with respect to the (left) SIMPLEX_KBRO and (right) PCA_KBRO circulation centers.

bias in SIMPLEX_KBRO; therefore, more accurate GBVTD winds are expected from PCA_KBRO. This prediction is verified by qualitative and quantitative comparisons of Figs. 7 and 9c,d. There is better qualitative agreement of Fig. 9d compared to Fig. 9c, and there is a wind intensity bias of 4.3 and -0.49 m s^{-1} shown in Figs. 9c and 9d, respectively.

With the likely location of the true circulation center position narrowed down to near SIMPLEX_KCRP and PCA_KCRP, a reasonable assessment of the accuracy of the use of the proxy $\mathbf{V}_m \approx (u_s, v_s)$ can now be made— only the results using this proxy are currently available

TABLE 3. The difference between the GBVTD-area-averaged and the pseudo-triple-Doppler-radar-area-averaged (ground truth) along-beam component of the mean wind (ΔV_a), specific for each circulation center estimate and radar. Also shown are 99% confidence limits in ΔV_a. Theoretically, the circulation center closest to the true circulation center should have ΔV_a closest to zero as measured by both KBRO and KCRP. All units are in m s^{-1}.

Circulation center	KBRO	KCRP
SIMPLEX_KCRP	-1.5 ± 1.5	0.0 ± 1.4
PCA_KCRP	-1.4 ± 1.4	-0.3 ± 1.3
PCA_KBRO	-2.6 ± 1.8	0.9 ± 1.2
SIMPLEX_KBRO	2.5 ± 1.1	-5.0 ± 1.5

in real time at TPC. Comparing Figs. 7 and 8a,b, one can conclude that only a reasonable estimate of the magnitude of the wind maximum (intensity) can be achieved, not an estimate of the instantaneous phase of the wind maximum. Unfortunately, Fig. 9a compares more favorably with Fig. 7 despite the fact that SIMPLEX_KBRO is not likely nearest to the true circulation center. Therefore, given an accurate estimate of the circulation center position, Figs. 8a,b illustrate that real-time, mean-wind estimators are needed for use with GBVTD.

Figure 10 shows the complete GBVTD results from the KCRP and KBRO 1.5-km CAPPI maps using *just* the SIMPLEX_KCRP circulation center. The left-hand side shows results where V_{T0} has *not* been corrected for the across-beam component of $\mathbf{V}_m \approx (u_m, v_m)$, whereas the right-hand side shows same results with this correction as per (1). Figures 10a,b show the GBVTD V_{T0} magnitude. Figures 10c,d and 10e,f show the ground-relative GBVTD wind speed derived from the KCRP and KBRO data, respectively. The sign of the correction to V_{T0} for KBRO is opposite to that for KCRP because of the ~180° difference in θ_T used in (1); for example, winds decrease (increase) in going from Fig. 10c to 10d (Fig. 10e to 10f). Clearly, the effect of the correction
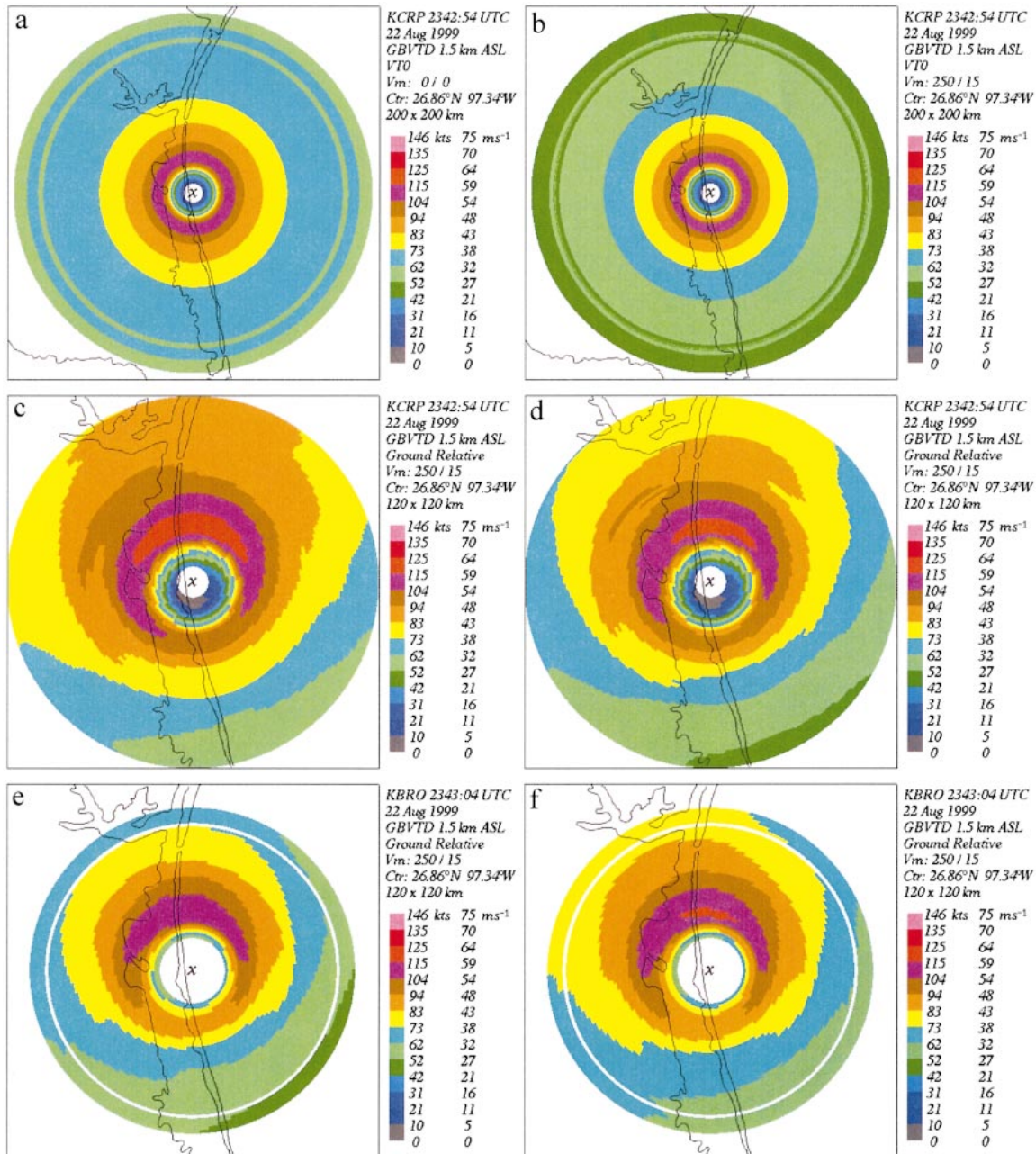
Fig. 10. GBVTD results at 1.5-km ASL using the SIMPLEX_KCRP circulation center (Fig. 6a) indicated by an ''x'' at the center of each display. (left) Results in which V_{T0} has *not* been corrected for the across-beam component of $\mathbf{V}_m$, and (right) the same results with this correction as per Eq. (1). Here $\mathbf{V}_m$ is expressed as meteorological azimuth direction, and speed is in kt (15 kt $\approx$ 7.6 m s^{-1}). (a), (b) depict V_{T0} calculated from the KCRP data over a 200 km $\times$ 200 km area; (c), (d) the ground-relative wind speed calculated from the KCRP data over a 120 km $\times$ 120 km area; and (e), (f) same as (c) and (d), except calculated from the KBRO data.

is noticeable at all radii from the RMW and outward; for example, the radius of 32 m s^{-1} winds changes by ~32 km between Fig. 10a and 10b. Note that Figs. 10d,f show good agreement between KCRP and KBRO, which further supports the accuracy of SIM-PLEX_KCRP.

TREC was applied to CAPPI maps of reflectivity and Doppler velocity from KCRP at 2342:54 and 2347:54

UTC (not shown) and from KBRO at 2343:04 and 2348:58 UTC (not shown). A grid spacing of 5 km was used in the analyses. Owing to the different geometries between Bret and the two radars, 1.5- and 2.25-km CAPPI maps were utilized from KCRP and KBRO. The lack of data on the north side of Bret shown in the 1.5-km CAPPI maps for KBRO (Figs. 5a,b) did not permit a complete TREC result around the area of maximum

winds, and a 2.25-km CAPPI was chosen to coincide with the next-available pseudo-triple-Doppler wind results at 2.25-km altitude. These results (not shown) are very similar to those shown in Fig. 7 except the wind maximum is 0.4 m s^{-1} smaller. To demonstrate the effect of using different wind center estimates, Fig. 11 shows the TREC results for Hurricane Bret using a polar coordinate system centered on the NHC_FIX (left) and AF_RECON (right) wind centers. Figures 11a,b show winds derived from the 2.25-km CAPPI maps for KBRO and the Figs. 11c,d show winds derived from the 1.5-km CAPPI maps for KCRP. The apparent intensity of Bret decreases on the north side of the eyewall when the wind center is moved from NHC_FIX to AF_RECON in both the KCRP and KBRO results. Therefore, the choice of origin in the polar coordinate system seems to have a notable effect on the TREC results. Comparing these results to Fig. 7, one can conclude that TREC estimates the magnitude and region of maximum winds reasonably well despite the noisy appearance of the results. The weak winds on the north side of Figs. 11a,b are likely due to the regions of weak reflectivity echoes shown in Fig. 5c. The trough of low wind speeds extending south of Bret's eye shown in Figs. 11a–d is due to the superposition of the zero isodop shown in Figs. 5d,f where the winds resulting from the reflectivity alone were weak and are thus not improved by the inclusion of the Doppler velocity. This problem was more widespread in the TREC analyses using a Cartesian coordinate system for both KCRP and KBRO (not shown), to the extent that almost the entire estimated wind field was a reflection of the dipole structure in the Doppler velocity pattern (TREC wind vectors derived from reflectivity data alone appeared randomly oriented and weak). Clearly, some or all of the potential problems that can affect TREC (section 3b) occurred in Bret. However, unlike the findings of TG, poor results were not restricted to the eyewall and rainband regions. Therefore, these results support the conjecture of TG that there is an advantage in using a polar coordinate system when the Cartesian version of TREC produces poor results in intense TCs.

b. Tropical Storm Barry (2001)

Barry was a tropical storm on the threshold of becoming a hurricane when it made landfall along the Florida panhandle on 6 August 2001. The Elgin Air Force Base (KEVX) WSR-88D observed Barry as it moved toward 10° azimuth at a speed of 3.6 m s^{-1}. Figure 12 shows the 16-contour-level display data of reflectivity at 0221:02 UTC and Doppler velocity at 0225:58 UTC derived from the KEVX 0.5° PPI scan, which were received at TPC in real time. Eight-contour-level Doppler velocity data were not necessary in this case since the 16-contour-level data represented the wind field well. Owing to data flow problems during the initial implementation of the method shown in Fig.

1, a complete set of data were not available at all times. TREC was applied to the 3.0-km CAPPI maps of reflectivity and Doppler velocity derived from the PPI display data at 0221:02 and 0225:58 UTC, whereas GBVTD was applied to the 3.0-km CAPPI map of Doppler velocity derived from the PPI display data at 0225:58 UTC (e.g., Figs. 13a,b). These two different times were chosen where enough data were received to make the necessary CAPPI maps for complete GBVTD and TREC analyses nearest to the AF_RECON estimate taken at 3.0-km altitude at 0227:00 UTC. In addition, only the two (three) lowest elevation angle PPI display data were available to construct the CAPPI maps of reflectivity (Doppler velocity); thus, the reason for the larger missing data circle over the radar in Fig. 13a compared to Fig. 13b. Figure 13c shows the AF_RECON wind center estimate relative to another wind center estimate denoted by "CAPPI_FIX," which was derived from the 3.0-km CAPPI maps at 0225:58 UTC using the same technique described above for NHC_FIX but without animation (an actual NHC_FIX was not available at this time). As in this case, it is quite common to find the wind center closer to the eyewall reflectivity maximum, especially in asymmetric storms such as Barry (Marks 1990). The simplex and PCA methods were applied to the CAPPI data shown in Fig. 13b and yielded two independent circulation center estimates whose relative positions are also indicated in Fig. 13c as "SIMPLEX" and "PCA." SIMPLEX utilized an initial RMW estimate of 30 km and the CAPPI_FIX as the initial center guess. Figure 13c also shows error bars and uncertainty circles that were determined in the same way as those described for Bret above. The perimeter of Fig. 13c is shown superimposed on Figs. 13a,b. Table 2 shows the coordinates of all of these center estimates. The large uncertainty radius for AF_RECON indicates that it was difficult to estimate the wind center position within a broad region of light and variable winds. The extensive data gaps around the eye region resulted in relatively larger error bars for SIMPLEX and PCA in this case compared to those found in Bret.

Air Force reconnaissance wind observations recorded at 3-km altitude between 0135:00 and 0250:00 UTC (hereafter, recon winds) were used to verify the GBVTD- and the TREC-estimated winds. Figure 14a shows the GBVTD ground-relative wind speed at 0225:58 UTC using the SIMPLEX circulation center and the storm motion as a proxy for the mean wind. Figure 14b shows the same wind speeds, except using the PCA circulation center. Figures 14c,d show the results of Figs. 14a,b over a larger 200 km × 200 km domain for comparison with the TREC results, with the recon winds superimposed at 2-min intervals (actual wind observations are within approximately ±1.5 m s^{-1} of the wind barb values). Allowing for the possibility of wind evolution over the time of the recon winds—and the differences between the point measurements of the recon versus the regionally smoothed Fourier analyses in-
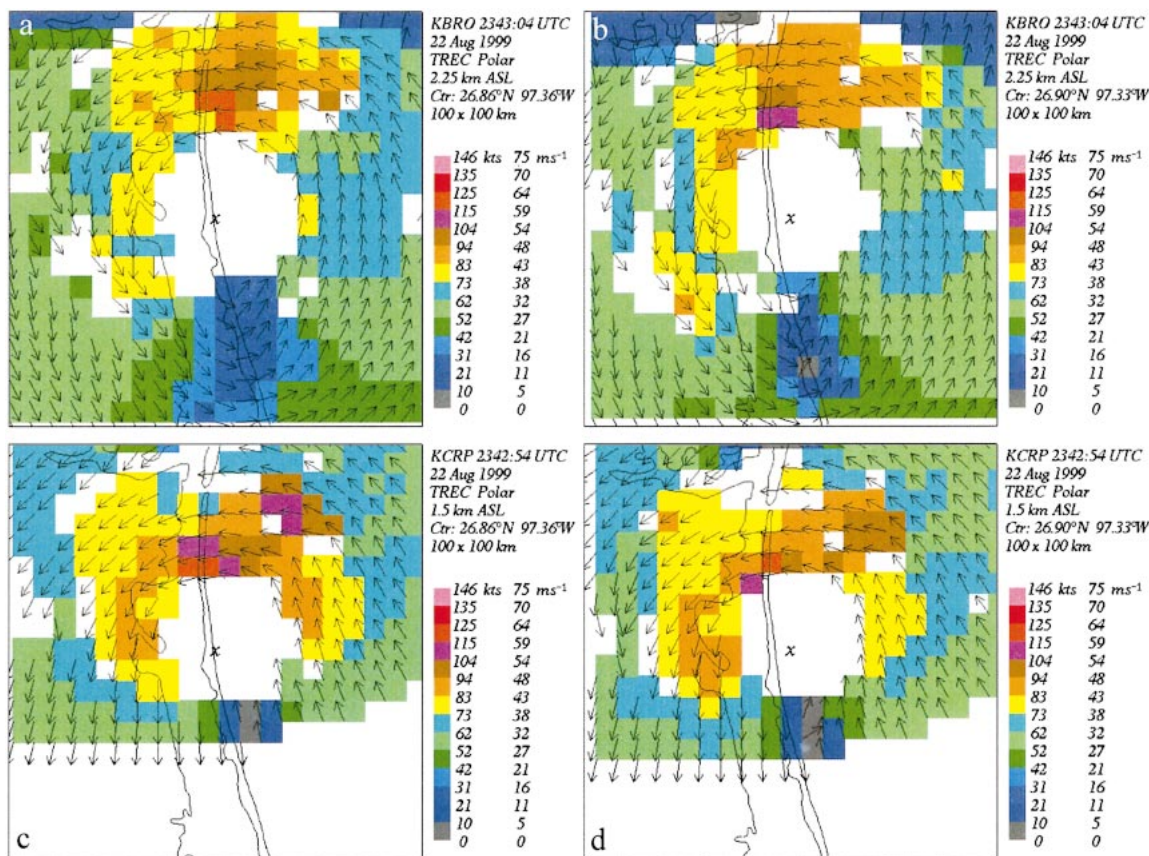
FIG. 11. TREC analyses using a polar coordinate system centered at the (left) NHC_FIX and (right) AF_RECON wind centers. Wind directions and speeds were calculated using a 5-km grid spacing and are indicated by arrows and the color bar, respectively. (top) Winds derived from the 2.25-km reflectivity and Doppler velocity CAPPI maps for KBRO, and (bottom) winds derived from the 1.5-km reflectivity and Doppler velocity CAPPI maps for KCRP. The area shown in each case is 100 km × 100 km centered at the center position indicated, with the geographical boundaries overlain for comparison with Fig. 7. An "x" marks the location of the wind centers used (also shown in Fig. 6a).

volved in GBVTD—the GBVTD results in Figs. 14a–d agree reasonably well with the recon winds. Maximum wind speeds of 33.95 m s^{-1} were reported in the recon winds in the northeast quadrant at 0156:00 UTC (not shown), which agree with the orange-colored regions in Figs. 14a–d. Therefore, the mean-wind proxy appears to have worked satisfactorily for Barry.

Figure 14e shows the TREC winds at 0221:02 UTC using a grid spacing of 5 km and a polar coordinate system centered on the CAPPI_FIX wind center. Figure 14f shows the same winds, except using a polar coordinate system centered on the AF_RECON wind center. As in the case of Hurricane Bret, there are notable changes in the TREC results when moving the polar coordinate origin from the CAPPI_FIX to the AF_RECON wind centers. The problem of data coverage was also an issue for Barry, as suggested by the weak TREC winds on the south side of the large data gap surrounding KEVX at 3-km altitude. However, the overall wind structure of the TREC results agrees well with the recon winds. Comparing the GBVTD and TREC results, one sees the valuable wind information

offered by TREC at ranges beyond the reach of GBVTD. We note in passing that, in contrast to the situation with Bret, TREC results similar to Fig. 14e were also obtained using a Cartesian coordinate system (not shown); therefore, none of the problems mentioned in section 3b were significant factors for the case of Barry. Since Barry was significantly less intense than Bret, the previous conclusion of TG that problems in the Cartesian version of TREC usually occur with more intense TCs has been further supported by the results of this study.

c. Skill assessment

Currently at TPC/NHC, there is no means to determine the most accurate circulation and wind center estimate provided by the various center-finding techniques in real time. In addition, the situation presented by Hurricane Bret was rare from the standpoint of having two radars optimally positioned to observe a TC simultaneously. Thus, having four circulation center estimates available for "a consensus of the majority" approach in determining the best estimate is also a rare occur-
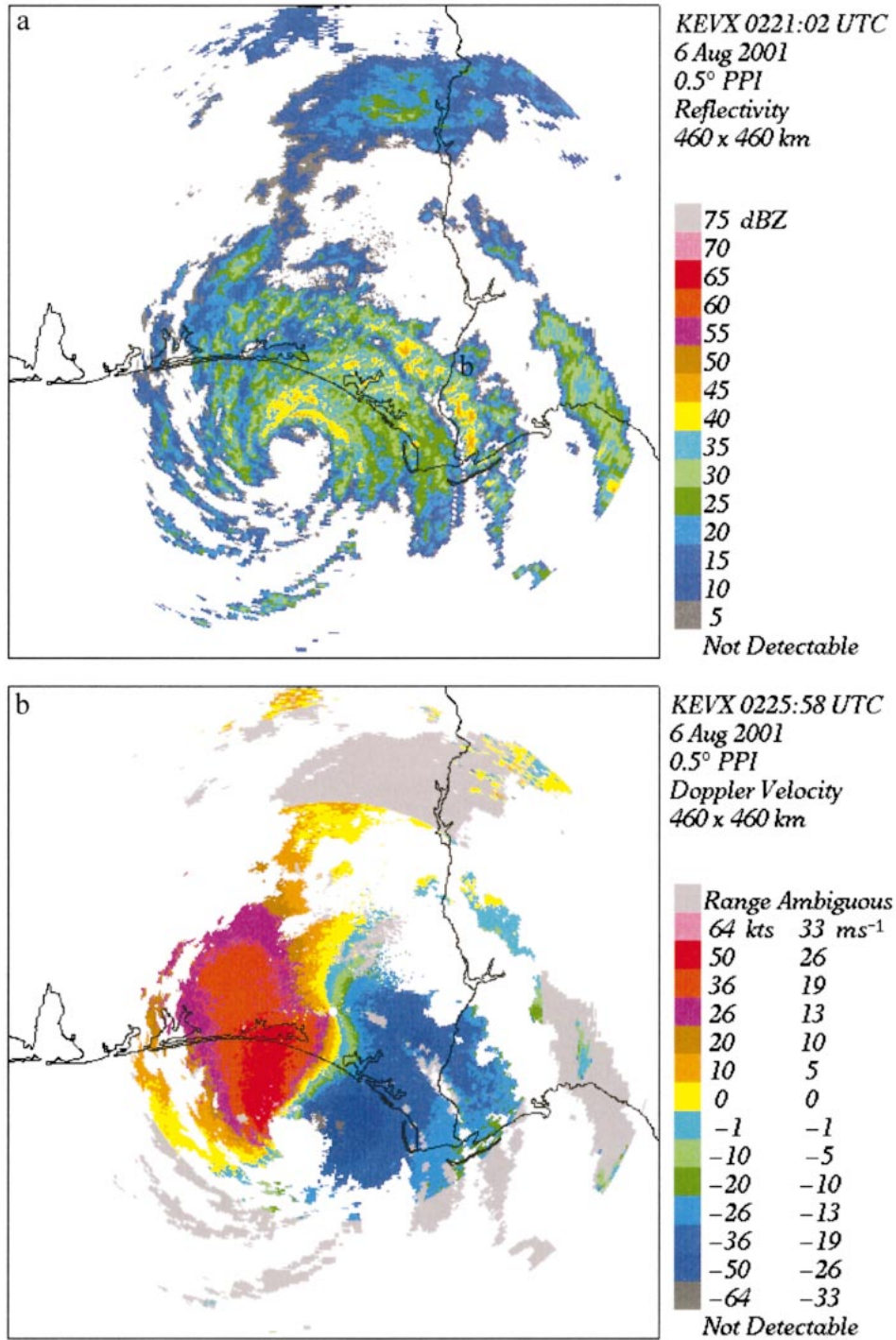
Fig. 12. The 16-contour-level PPI maps at 0.5° elevation showing Tropical Storm Barry as it made landfall along the Florida panhandle near the KEVX radar on 6 Aug 2001. The maps show a 460 km × 460 km area centered on KEVX: (a) reflectivity at 0221:02 UTC and (b) Doppler velocity at 0225:58 UTC.

rence. However, despite these shortcomings, the foregoing results demonstrate a degree of skill in the ability of GBVTD and TREC to accurately estimate the intensity (maximum wind speed) of TCs, regardless of center-accuracy knowledge.

Figure 15 shows the intensity bias that would have resulted from the results shown in this paper, assuming that only *one* radar observed the particular TC and that the best individual GBVTD and TREC intensity estimates are those derived from an average of all the in-
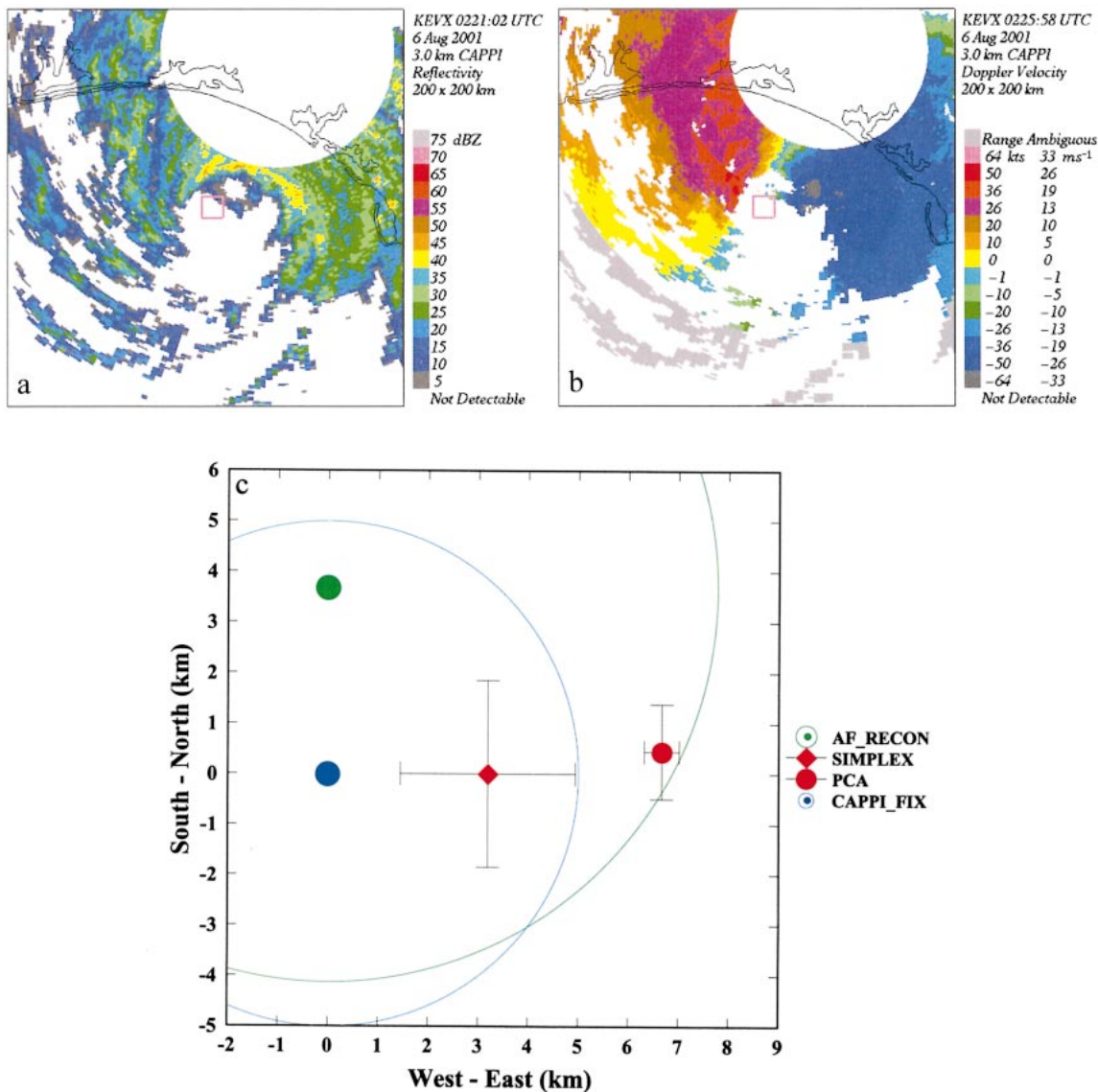
FIG. 13. (a) The 3.0-km CAPPI map of reflectivity derived from the 16-contour-level display data at 0221:02 UTC covering a 200 km × 200 km area centered on CAPPI_FIX. (b) Same as (a), except Doppler velocity at 0225:58 UTC. (c) The center fixes available for Tropical Storm Barry relative to the CAPPI_FIX at 3-km altitude. Circulation center estimates are shown as red symbols and black error bars, with labels shown in the legend indicating the technique used. Wind center estimates are shown as blue and green solid circles partially circumscribed by circles of the same color representing the approximate extent of their uncertainties. The location of the perimeter of (c) is delineated on (a) and (b) by pink-colored squares.

tensities' estimates available from each method. The skill is based on comparisons with the intensity measured by the aforementioned verification datasets. Note that if averages are not taken, then the biases from individual center results for Bret and Barry are *up to* a factor of ~2 larger than those shown in Fig. 15. Based on the average skill assessment approach, both the GBVTD and TREC algorithms were able to provide an estimate of the intensity of Hurricane Bret and Tropical Storm Barry with an accuracy of ~2 m s^{-1} or better. This would be invaluable information to TC forecasters and meets the TPC/NHC requirements for TC intensity

estimation via land-based Doppler radar (See http://www.nhc.noaa.gov/about88d.html for details). Furthermore, this knowledge *could not* have been estimated from the extreme Doppler velocities shown in the display data for Hurricane Bret; for example, analyses of Figs. 4e,f yield an intensity bias of −8.96 m s^{-1}. Note that Fig. 15 includes GBVTD results assuming an estimate of the mean wind had been available in real time for Bret. If accuracy probabilities of the two available circulation center estimates had also been utilized, then the GBVTD (V_m) bias for KBRO would be only −0.49 m s^{-1}.
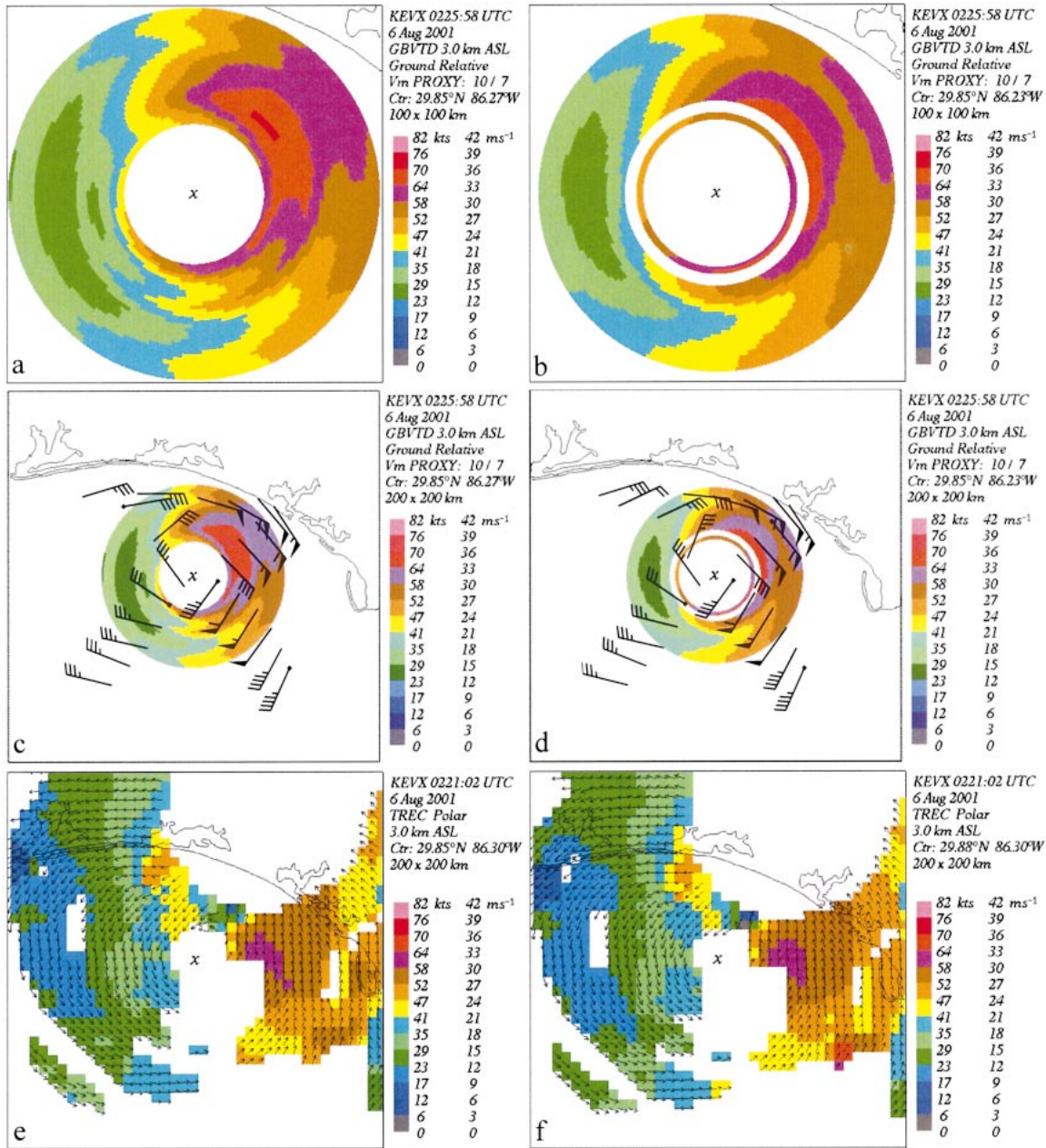
FIG. 14. (a) GBVTD ground-relative wind speed at 3.0-km altitude and at 0225:58 UTC using the SIMPLEX circulation center and the storm motion (10° azimuth, 3.6 m s^{-1}) as a proxy for the mean wind. (b) Same as (a), except using the PCA circulation center. (c) Same as (a), except over a 200 km × 200 km domain and overlain with recon winds observed at 3-km altitude between 0135:00 and 0250:00 UTC. Recon winds have been translated to their hypothetical position at 0225:58 UTC using the storm motion (flag = 25.7 m s^{-1}; full barb = 5.1 m s^{-1}; half barb = 2.6 m s^{-1}). (d) Same as (c), except for the results shown in (b). (e) TREC winds at 3.0-km altitude and at 0221:02 UTC using a polar coordinate system centered at the CAPPI_FIX wind center. Winds are shown along a 5-km grid spacing and are indicated by arrows and the color bar. (f) Same as (e), except using the AF_RECON wind center. An "x" marks the location of the center used in each case (also shown in Fig. 13c).

5. Summary and conclusions

New and improved methods have been presented for using WSR-88D display data as a proxy for full-resolution base data that are required by single-Doppler radar algorithms for TC wind field retrieval and center finding. Algorithms currently being evaluated at TPC are the GBVTD, simplex, TREC, and PCA methods. Display data are sent from the WSR-88D RPG to AWIPS at TPC. CAPPI maps are constructed from the display data and then input into the algorithms at an adjacent workstation. NOAA/NWS is currently expanding the CRAFT project and transitioning its infrastruc-
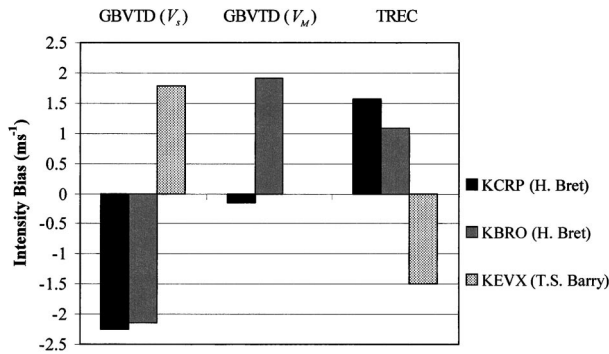
FIG. 15. Bias in the GBVTD and TREC intensity (max wind speed) found for Hurricane Bret and Tropical Storm Barry. Results are shown across the three categories (algorithms) GBVTD (V_S), GBVTD (V_M), and TREC for the three series (radars) KCRP, KBRO, and KEVX. The V_S signifies the use of the storm motion as a proxy for the mean wind whereas V_M signifies the use of the mean wind (which was only available for Hurricane Bret). GBVTD-estimated intensities using the simplex and PCA circulation centers have been averaged in each case. Similarly, TREC-estimated intensities using the two wind center estimates at the analysis altitude have been averaged. For the case of Hurricane Bret, skill is measured against the max wind in the triple-Doppler results at 1.5-km altitude shown in Fig. 7 (60.4 m s^{-1}) for all results except the KBRO TREC result, which uses the max winds at 2.25-km altitude not shown (60.0 m s^{-1}). For the case of Tropical Storm Barry, the max flight level wind of 33.95 m s^{-1} found by the recon winds in the northeast quadrant at 0156:00 UTC is used to access skill.

ture to a NWS-based system so that most WSR-88D units located in the continental United States are delivering base data to regional servers in near–real time (greater than 95% reliability) by the end of 2004 (T. D. Crum 2003, personal communication). Therefore, we view the use of display data as not only an interim solution but also as a permanent recourse for those occasions when base data are not available.

Improvements to the GBVTD and TREC algorithms have been developed and implemented at TPC. The mean-wind-relative GBVTD winds are transformed to the more operationally useful, ground-relative winds by using the storm motion as a proxy for the mean wind. The across-beam component of the storm motion is used both in the transformation to the ground-relative frame of reference and in a correction for V_{T0}. Both corrections are needed in order to accurately estimate the wind field. GBVTD requires an estimate of the circulation center position that is obtained from both the simplex and PCA methods. There are also some new processing techniques applied to GBVTD based on empirical and theoretical considerations. Polar and Cartesian coordinate versions of the TREC algorithm have been implemented in real time at TPC. Whereas the origin of the Cartesian coordinate version is the radar, the origin of the polar coordinate version is the wind center, which is estimated by either display data or aircraft reconnaissance data.

The operational versions of GBVTD and TREC were applied with substantial success to WSR-88D display data of Hurricane Bret (1999) and Tropical Storm Barry

(2001). Results from Bret were compared with a pseudo-triple-Doppler wind analysis, which afforded an ideal opportunity to test both the accuracy of the use of the storm motion as a proxy for the mean wind in GBVTD and the sensitivity of the GBVTD winds to the accuracy of the circulation center estimate. The test results illustrate that the proxy provided the least-accurate estimate of the wind field when using the most accurate circulation center estimates. However, the results also showed that having an accurate estimate of the mean wind and circulation center available for GBVTD in real time could provide TC forecasters with an accurate description of the entire TC wind field within radar range. The conjecture by TG that the use of the polar coordinate version of TREC could eliminate problems arising from the use of the Cartesian coordinate version with intense storms has been supported in the TREC results for Bret. In addition, it was demonstrated that the use of different wind center estimates had a notable effect on the results for both Bret and Barry. The GBVTD and TREC wind estimates for Barry agreed reasonably well with the recon winds. The Bret and Barry results together suggest that both GBVTD and TREC have the ability to retrieve the intensity of a TC with an accuracy of ~2 m s^{-1} or better when all the individual results are averaged together.

This work represents a major step toward building a complementary suite of algorithms that diagnose the TC wind field in real time. Although the results derived from display data are very encouraging, more verification studies are needed to confirm the major findings of this research. The use of real-time base data at TPC/NHC in the near future should further improve the performance of the methods. Efforts are currently under way to utilize the single-Doppler radar techniques of Harasti (2003) and Bell and Lee (2002) that show promise in addressing the problems of mean-wind estimation and confidence levels in circulation center estimates, respectively. Future research should include impact studies on the assimilation of the methods' results into the HRD surface wind field analyses (Powell et al. 1996) and NWP models for TCs.

REFERENCES

Baer, V. E., 1991: The transition from the present radar dissemination system to the NEXRAD Information Dissemination Service (NIDS). *Bull. Amer. Meteor. Soc.,* **72,** 29–33.

Bell, M. M., and W.-C. Lee, 2002: An objective method to select a consistent set of tropical cyclone circulation centers derived from the GBVTD-simplex algorithm. Preprints, *25th Conf. on Hurricanes and Tropical Meteorology,* San Diego, CA, Amer. Meteor. Soc., 642–643.

Browning, K. A., and R. Wexler, 1968: The determination of kinematic properties of a wind field using Doppler radar. *J. Appl. Meteor.,* **7,** 105–113.

Crum, T. D., R. L. Alberty, and D. W. Burgess, 1993: Recording, archiving, and using WSR-88D data. *Bull. Amer. Meteor. Soc.,* **74,** 645–653.

——, R. E. Saffle, and J. W. Wilson, 1998: An update on the NEXRAD program and future WSR-88D support to operations. *Wea. Forecasting,* **13,** 253–262.

Dodge, P. P., M. L. Black, J. L. Franklin, J. F. Gamache, and F. D. Marks, 2002: High-resolution observations of the eyewall in an intense hurricane: Bret on 21–22 August 1999. Preprints, *25th Conf. on Hurricanes and Tropical Meteorology,* San Diego, CA, Amer. Meteor. Soc., 607–608.

Donaldson, R. J., Jr., and F. I. Harris, 1989: Estimation by Doppler radar of curvature, diffluence, and shear in cyclonic flow. *J. Atmos. Oceanic Technol.,* **6,** 26–35.

Droegemeier, K. K., and Coauthors, 2002: Project CRAFT: A test bed for demonstrating the real time acquisition and archival of WSR-88D level II data. Preprints, *18th Int. Conf. on Interactive Information and Processing Systems for Meteorology, Oceanography, and Hydrology,* Orlando, FL, Amer. Meteor. Soc., 136–139.

Elsberry, R. L., and F. D. Marks, 1998: U.S. Weather Research Program Hurricane Landfall Workshop Report. NCAR Tech. Note TN-442 + PROC, 40 pp.

Emanuel, K., and Coauthors, 1995: Report of the first prospectus development team of the U.S. Weather Research Program to NOAA and the NSF. *Bull. Amer. Meteor. Soc.,* **76,** 1194–1208.

Gamache, J. F., 1997: Evaluation of a fully three-dimensional variational Doppler analysis technique. Preprints, *28th Conf. on Radar Meteorology,* Austin, TX, Amer. Meteor. Soc., 422–423.

Harasti, P. R., 2000: Hurricane properties by principal component analysis of Doppler radar data. Ph.D. dissertation, University of Toronto, 162 pp.

——, 2003: The hurricane volume velocity processing method. Preprints, *31st Conf. on Radar Meteorology,* Seattle, WA, Amer. Meteor. Soc., 1008–1011.

——, and R. List, 2001a: Nowcasting hurricane properties by principal component analysis of Doppler velocity data. Preprints, *30th Conf. on Radar Meteorology,* Munich, Germany, Amer. Meteor. Soc., 255–258.

——, and ——, 2001b: The hurricane-customized extension of the VAD (HEVAD) method: Wind field estimation in the planetary boundary layer of hurricanes. Preprints, *30th Conf. on Radar Meteorology,* Munich, Germany, Amer. Meteor. Soc., 463–465.

Houston, S. H., G. Forbes, A. Chiu, W.-C. Lee, and P. P. Dodge, 1999: Super Typhoon Paka's (1997) surface winds. Preprints, *23rd Conf. on Hurricanes and Tropical Meteorology,* Dallas, TX, Amer. Meteor. Soc., 1032–1033.

Lee, W.-C., and F. D. Marks, 2000: Tropical cyclone kinematic structure retrieved from single Doppler radar observations. Part II: The GBVTD-simplex center finding algorithm. *Mon. Wea. Rev.,* **128,** 1925–1936.

——, B. J.-D. Jou, P.-L. Chang, and S.-M. Deng, 1999: Tropical cyclone kinematic structure retrieved from single Doppler radar observations. Part I: Interpretation of Doppler velocity patterns and the GBVTD technique. *Mon. Wea. Rev.,* **127,** 2419–2439.

——, ——, ——, and F. D. Marks, 2000: Tropical cyclone kinematic structure retrieved from single Doppler radar observations. Part III: Evolution and structures of Typhoon Alex (1987). *Mon. Wea. Rev.,* **128,** 3982–4001.

Marks, F. D., Jr., 1990: Radar observations of tropical weather systems. *Radar in Meteorology,* D. Atlas, Ed., Amer. Meteor. Soc., 401–425.

——, and L. K. Shay, 1998: Landfalling tropical cyclones: Forecast problems and associated research opportunities. *Bull. Amer. Meteor. Soc.,* **79,** 305–323.

——, R. A. Houze, and J. Gamache, 1992: Dual-aircraft investigation of the inner core of Hurricane Norbert. Part I: Kinematic structure. *J. Atmos. Sci.,* **49,** 919–942.

Marshall, J. S., 1957: The constant altitude presentation of radar weather patterns. *Proc. Sixth Weather Radar Conf.,* Boston, MA, Amer. Meteor. Soc., 321–324.

McAdie, C. J., P. R. Harasti, P. P. Dodge, W.-C. Lee, S. T. Murillo, and F. D. Marks Jr., 2001: Real-time implementation of tropical cyclone–specific radar data processing algorithms. Preprints, *30th Conf. on Radar Meteorology,* Munich, Germany, Amer. Meteor. Soc., 466–468.

Mohr, C. G., L. J. Miller, R. L. Vaughan, and H. W. Frank, 1986: The merger of mesoscale datasets into a common Cartesian format for efficient and systematic analyses. *J. Atmos. Oceanic Technol.,* **3,** 143–161.

Powell, M. D., S. H. Houston, and T. A. Reinhold, 1996: Hurricane Andrew's landfall in South Florida. Part I: Standardizing measurements for documentation of surface wind fields. *Wea. Forecasting,* **11,** 304–328.

Rinehart, R. E., and E. T. Garvey, 1978: Three-dimensional storm motion by conventional weather radar. *Nature,* **273,** 287–289.

Stidd, C. K., 1967: The use of eigenvectors for climatic estimates. *J. Appl. Meteor.,* **6,** 255–264.

Tuttle, J. D., and G. B. Foote, 1990: Determination of the boundary layer airflow from a single Doppler radar. *J. Atmos. Oceanic Technol.,* **7,** 218–232.

——, and R. Gall, 1999: A single-radar technique for estimating the winds in tropical cyclones. *Bull. Amer. Meteor. Soc.,* **80,** 653–668.

Willoughby, H. E., 1992: Linear motion of a shallow-water barotropic vortex as an initial-value problem. *J. Atmos. Sci.,* **49,** 2015–2031.

——, and M. E. Rahn, 2002: A new parametric model of hurricane wind profiles. Preprints, *25th Conf. on Hurricanes and Tropical Meteorology,* San Diego, CA, Amer. Meteor. Soc., 553–554.